جامعــة خليفـة
Khalifa University

Numerical Study of Liquid-Liquid Slug Flow Hydrodynamics in Serpentine Microchannel for Biodiesel Production Intensification

Azeeza Naser Alrashdi

MSc. Thesis

December 2023

جامعــة خليفــة
Khalifa University

Numerical Study of Liquid-Liquid Slug Flow Hydrodynamics in Serpentine Microchannel for Biodiesel Production Intensification

by

Azeeza Naser Alrashdi

A thesis submitted in partial fulfillment of the

requirements for the degree of

Master of Science in Chemical Engineering

at

Khalifa University

Thesis Committee

Dr. Nahla Alamoodi (Main Advisor),

Khalifa University

Dr. Cheng Chin Kui (RSC Member 1),

Khalifa University

Dr. Abdulla Berrouk (Co-Advisor)

Khalifa University

Dr. Anas Alazzam (RSC Member 2),

Khalifa University

December 2023

Abstract

Azeeza Naser Alrashdi, "**Numerical Study of Liquid-Liquid Slug Flow Hydrodynamics in Serpentine Microchannel for Biodiesel Production Intensification**", M.Sc. Thesis, Master of Science in Chemical Engineering, Department of (Chemical & Petroleum Engineering), Khalifa University of Science and Technology, United Arab Emirates, December 2023.

Biodiesel is highly considered within the industrial and research field because of its high heating value, which enables it to be an excellent alternative to fossil fuels such as petroleum diesel [1]. Studies showed that utilizing microfluidic devices for biodiesel transesterification is highly recommended to replace the mechanically stirred batch reactors where the mass transfer is considered low, and the mixing time is very long [2]. Employing a Slug-based serpentine microchannel will enable stronger internal circulations, which means higher vorticity and consequently enhances the mixing efficiency for biodiesel production intensification. Therefore, this work investigates numerically the hydrodynamics of a slug flow pattern in several serpentine microchannels for biodiesel production intensification using the Volume of Fluid (VOF) method. A straight microchannel was also simulated to compare the impact of the geometry configuration on vorticity. Also, for serpentine microchannels, the impact of the geometrical dimensions (i.e., width, corner shape, and curvature radius) and operational parameters (i.e., alcohol-to-oil ratio) was examined to optimize the microchannel performance. The results showed that the serpentine microchannel achieved higher vorticity by 233% compared to the straight microchannel. The smaller width was found to be better using Dean Number analysis and vorticity measurement. Also, the 90-degree corner shape was found to induce slightly higher vorticity than the rounded shape due to the increment of the unbroken internal circulations because of the sharp intrusion.

Moreover, the longer the curvature radius, the better the vorticity. The very short radius caused over-deformation of the internal circulation that weakened vorticity. Regarding the effect of the molar ratio, the 7.6 molar ratio resulted in a higher number of slugs falling in the range of L/D between 2.3 and 6 compared to the 22.9 molar ratio. The mentioned slug L/D range results in the highest vorticity compared to the vorticity produced by other ranges (i.e., L/D<2.3 and L/D>6) in the 22.9 molar ratio.

Indexing Terms: Slug, Serpentine Microchannel, Vorticity, Internal Circulation, Hydrodynamics, Molar ratio, Dean Number, Biodiesel, VOF.

Acknowledgment

First, Alhamdulillah (Praise be to Allah the Almighty) for the ease he provided me to attain this accomplishment.

Second, I would like to express my sincere gratitude to my beloved country, the United Arab Emirates, for establishing such a great university as Khalifa University and for fostering the country's youth to learn and excel to serve the nation. It is an Honor indeed.

Also, I would like to thank my main advisor, Dr. Nahla Alamoodi, for her consistent support and guidance while running this project. In addition to her broad academic knowledge, her kindness and compassion made me look at her not only as my main advisor but also as a role model to follow in life. Thank you, a lot.

I also would like to acknowledge and thank Dr. Abdulla Berrouk (Co-Advisor), Dr. Annas Alazzam, Dr. Cheng Chin Kui (RSC member) as well as Dr. Elie Ayoub from the Chemical Engineering Department for all the support they provided me through my thesis preparations.

Lastly, my parents Naser Mohamed Alrashdi & Norh Ahmed Haimed, no words of gratitude can express enough how much I'm grateful to have you and my siblings in my life. You are the true meaning of family.

Declaration and Copyright

Declaration

I declare that the work in this thesis was carried out in accordance with the regulations of Khalifa University of Science and Technology. The work is entirely my own except where indicated by special reference in the text. Any views expressed in the thesis are those of the author and in no way represent those of Khalifa University of Science and Technology. No part of the thesis has been presented to any other university for any degree.

Author Name: Azeeza Naser Alrashdi

Author Signature:

Date: 11th December 2023

Copyright ©

Contents Table

List of Figures

List of Tables

List of Abbreviations

Volume of Fluid	VOF
Sodium hydroxide	NaOH
Potassium hydroxide	KOH
Computational Fluid Dynamics	CFD
Mixing Static Elements	MSE
Tubular Microreactor	TMR
Left Hand Side	LHS
Right Hand Side	RHS
Length To Diameter Ratio	L/D

Chapter 1: Introduction

1.1   Biodiesel Overview

Biodiesel is a mixture of alkyl esters that is used as an alternative to fossil fuels such as petroleum diesel. This non-toxic fuel is considered within the industrial and research field because of its biodegradability, fewer emissions, and renewability. It can even be used in the current diesel engine without significant modifications [1]. Many techniques are utilized to produce biodiesel, such as emulsification, simple mixing, and transesterification [3], which is the most commercially adopted one. The reactants used are triglycerides and alcohol. Triglycerides could be extracted from edible and non-edible oils, waste cooking oil, and animal fats. Methanol and ethanol are widely used to produce biodiesel mainly due to their availability and cost. The obtained products are biodiesel (i.e., alkyl ester) and glycerol, which is a by-product. Several factors can affect the transesterification process, which are alcohol-to-oil molar ratio, residence time, reaction temperature, and catalyst concentration. A large amount of alcohol (i.e., more than 3:1 of alcohol to triglycerides ratio) is required to keep the reaction producing biodiesel. Homogeneous alkaline catalysts (such as NaOH and KOH) are widely used to avoid the corrosive nature of the acidic homogenous catalysts and to avoid increasing temperature, pressure, and reaction time of the system, which could be very costly [4].

For biodiesel production, the reactor choice is crucial since it affects the mixing degree of the immiscible phases, the mass transfer, and the reaction rate of transesterification. Various novel reactors, such as oscillatory flow reactors and spinning tube reactors, are proposed for

transesterification to replace the mechanically stirred batch reactors where the mass transfer is considered low. The mixing time is very long (1 to 2 hours) [2], although stirred batch reactors are well known for their feedstock flexibility and less capital cost [5].

One of the potential alternatives is the use of micromixers in microfluidic platforms, which are small-length scale devices ranging from sub-micrometers to sub-millimeters. The past decade has shown much interest in microfluidic mixers because of their high efficiency, low cost, and high throughput when multiple microchannels are compiled. Many companies started to adopt micromixers, such as Corning and Ehrfeld Mikrotechnik BTS, by associating the micromixers with device parallelization and numbering-up approaches [6]. Microfluidic platforms are designed to increase the interface area or area-to-volume ratio and decrease the reactants' diffusion time, which will ensure proper mixing and high conversion. Micromixers are divided into two categories: active and passive micromixers. Active micromixers are used with an external force/field source to make the fluid flow behave in a particular manner, such as using ultrasound or electrowetting techniques. Conversely, Mixing in passive micromixers depends on the geometry (i.e., shape and dimensions) and flow properties to enhance the mixing [2]. Passive micro-mixers are characterized by their simplicity in fabrication and operation compared to their active counterparts. They operate without the need for external energy sources or extra components, making them straightforward to design and use. moreover, they are energy-efficient and ideal for low-power applications.

Herein, a numerical investigation of different geometries of serpentine microchannels with a slug-based flow was conducted to optimize a potential micromixer for biodiesel production intensification using Volume of Fluid (VOF). The hydrodynamics was enhanced by strengthening the vorticity of the internal circulations and adding chaotic advection, which is assumed

accordingly to help improve the mixing inside the slug and increase the conversion at the interface. The slug flow pattern was chosen because of its high area-to-volume ratio, which can increase the interfacial area between the reactants. The impact of the geometrical dimensions (i.e., width, corner shape, and curvature radius) and operational parameters (i.e., alcohol-to-oil ratio) was examined to optimize the best micromixer performance.

Chapter 2: Background and Literature Review

2.1 Simulation of Microfluidic Devices Performance for Biodiesel Production

Numerical analyses and computational fluid dynamics (CFD) simulations allow a comprehensive investigation of biodiesel production and mixing phenomena by predicting the effect of changing operating conditions and different geometry structures on the conversion. Santana et al. (2017) studied the mixing performance and triglycerides conversion to biodiesel in a microfluidic channel with mixing static elements (MSE). It was found that the highest observed mixing index was obtained at Re=100. While the highest oil conversion (91.53%) was noticed at a temperature of 75 °C, ethanol-to-oil molar ratio of 9, and catalyst concentration of 1% [7]. Terdsak et al. (2019) studied the effect of different operating conditions for both isothermal (pre-heating of reactants) and non-isothermal (without pre-heating) biodiesel reaction systems in a T-microchannel. Saponification was considered in the reaction kinetic model to enable the prediction of performance abnormalities due to any operating conditions deviations. The results showed very close ester yield outputs for the isothermal and non-isothermal cases for the following process parameters: temperature, alcohol/oil molar ratio, and residence time. One exception is the catalyst concentration, where the maximum yield for the isothermal case was obtained at 1% catalyst weight, while for the non-isothermal case, it was obtained at 1.5 %. It was claimed that as the catalyst weight increases while the temperature is changing, there is a competition between the transesterification and saponification reactions [8]. López-Guajardo et al. (2017) studied

numerically biodiesel production in Tubular Microreactor (TMR) with a slug flow pattern. The CFD was done to illustrate the interaction between the methanol and oil slugs in the TMR. In their model, the reaction kinetics were not considered; instead, two cases were simulated at 0% and 99% triglyceride conversion, illustrating the reaction's beginning and end. The scope of their numerical study was to investigate the change of the internal velocity with the change of density and viscosity of the slugs at different residence times. It is worth mentioning that in this study, the residence time resembles the linear velocity of the slugs. At 0% conversion, at low residence time, the internal velocity increases while the center of the stagnant zones in the methanol slug moves to the back interface. This is attributed to the low density and viscosity of the slug, resulting in inertial forces dominating viscous forces. At 99%, the methanol slug's internal velocity profile remains constant. This is due to the increase in the viscosity from glycerol formation, suggesting that the viscous forces dominate the inertial ones. In other words, the methanol slug's internal velocity profile did not change as the linear velocity increased because of the significance of the viscous forces with the 99% conversion compared to the 0% conversion. The oil slug's internal velocity was constant in both conversions due to the high viscous forces, which means that the oil slug was the main mass transfer limiting stage in both conversions [3]. Wei et al. 2011 explored the effect of a slug flow pattern on mixing efficiency in a capillary microreactor. A convective-diffusive-reactive model was solved, and the movement of the fluid was simulated, assuming moving walls and a slip boundary condition at the interface between the two phases. The simulation results were validated for the influence of the convective mixing since an increase in the average velocity led to a higher biodiesel concentration in a shorter residence time [9]. Afiq Laziz et al. (2020) investigated numerically the mixing performance within the methanol slug during the transesterification reaction in a T-junction capillary microreactor at room temperature.

Based on the 3D CFD simulation, the movement of the slug through the channel formed two major circulations at each side of the slug. The two circulations start moving from the front of the slug to the rear and then toward the center of the slug. This movement consequently creates a high-velocity profile in the center of the slug. Hence, it can be deduced that this high-velocity profile induces a force that pushes the slug faster along the channel than the oil continuous phase. Moreover, using the concentration profile resulting from the simulation, the change in the oil concentration within the methanol slug was investigated. High oil concertation was observed at the slug's front and rear due to the low velocity, indicating a low mass transfer. As time passes, the oil concentration increases inside the slug but remains negligible in the center of the circulation zones due to the low velocity in these zones [10]. In another study, Afiq Laziz et al. (2020) studied numerically a similar system as the previous one to explore the flow patterns produced and predict the size of the microdroplet in the microchannel considering the total volumetric flow rate and the oil to methanol volumetric ratio. It was observed that the segmented flow appeared at low volumetric flow rates at all the oil-to-methanol volumetric ratios. It was deduced that this could be due to the higher wettability of methanol with the channel wall at low flow rates. Another observation was that the droplet flow pattern was maintained better at a high oil-to-methanol volumetric ratio than the low ratios, even at a high total volumetric flow rate. Regarding the droplet size, it was observed that the droplet length is inversely proportional to the total volumetric flow rate and oil-to-methanol volumetric ratio. While the droplet flow pattern was found to have a high surface-to-volume ratio, this ratio varies as both the total volumetric flow rate and oil-to-methanol volumetric ratio vary. Droplets at a low oil-to-methanol volumetric ratio have a higher surface-to-volume ratio than a high oil-to-methanol volumetric ratio. Droplets at a lower oil-to-methanol

volumetric ratio have larger droplet areas and shorter distances between the droplets, which results in a high interfacial area at a small volume domain [11].

2.2 Slug-Flow in Serpentine Microchannels

Internal circulation and chaotic flow play a massive role in enhancing the mixing process in micromixers when they are integrated. Internal circulation inside the slug is generated because of the shear stress between the slug interface and the wall of the micromixer. Slug circulations can be major or minor circulations as depicted in Figure 1. Chaotic advection is created because of the deformation and rotation of the slug due to geometry manipulation, such as in serpentine microchannels. Geometrical changes can lead to asymmetrical circulation by stretching, folding, and rotation of the slug inside the micromixer, which significantly impacts mixing efficiency [12].
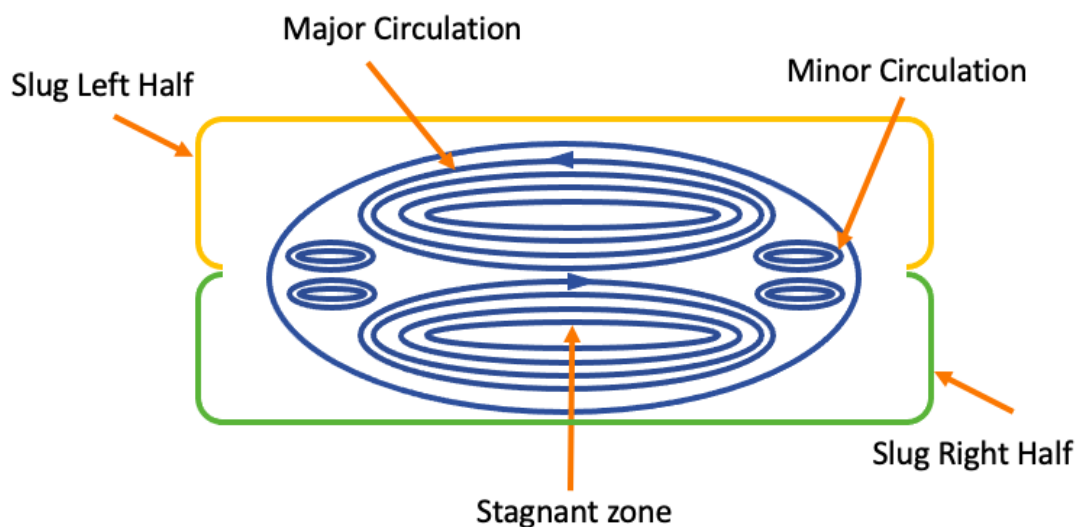
Figure 1 Internal Circulations Movement Within a Slug

Wang et al. (2015) studied the mixing hydrodynamic of oil and water in a circular serpentine microchannel with a slug flow pattern. Different circulation configurations were observed as the flow passes through the microchannel. Some were referred to as major circulations, and others as minor ones. These different circulations were located in different directions, dramatically controlling the mixing performance. Better mixing efficiency was found with the smallest droplet size since it does not require a long circulation period or mixing length to achieve a high mixing degree [13]. Masoud Madadelahi et al. (2017) discussed the mixing phenomena and chemical reactions of two reactant droplets flowing in a symmetrical serpentine microchannel. It was observed that the vorticity value and position change depending on the slug size and location. Additionally, it was found that the slug velocity magnitude increases after it passes through a bend [14]. Jin-yuan Qian et al. (2019) studied the mixing efficiency of two immiscible liquids in a serpentine microreactor as a function of the dispersed phase volume fraction and the bend radius. The increment of the dispersed phase fraction has a parabolic effect on the droplet frequency. Initially, when the dispersed fraction increased, the pressure accumulation increased, which caused a higher droplet breakup rate. However, a further increase in the dispersed fraction increased the droplet formation time, which decreased the droplet formation frequency. The highest droplet frequency was achieved with a dispersed phase fraction of 0.5. Thus, the dispersed phase fraction should be less than 0.5 to achieve high droplet formation frequency and mixing efficiency. Also, the study showed that the microchannels with the bend radius to channel width ratio of 0 (i.e., square corner) and 1 have a superior mixing efficiency compared to the higher ratios due to the

8

high dean number, which indicates a strong presence of secondary vortices around the bends with lower ratios [15]. Xiang Cao et al. (2006) investigated the droplet-based mixing in a circular symmetrical serpentine microchannel compared to other microchannel configurations. Figure 2 illustrates the effect of the serpentine geometry on the slug motion, where the large contact area between the droplet and the inside channel wall induces a robust shear force. The strong shear force and the centrifugal force resulted in a nonuniform fluid flow in the droplet. Moreover, due to the centrifugal force, the fluid motion concentrates mainly on the droplet's outward side, resulting in component A movement in the radial direction, wrapping component B simultaneously. At the same time, component A will be further entrained by the nonuniform, non-horizontal vortices of component B, which will cause a chaotic mixing that improves the droplet-based mixing [16].
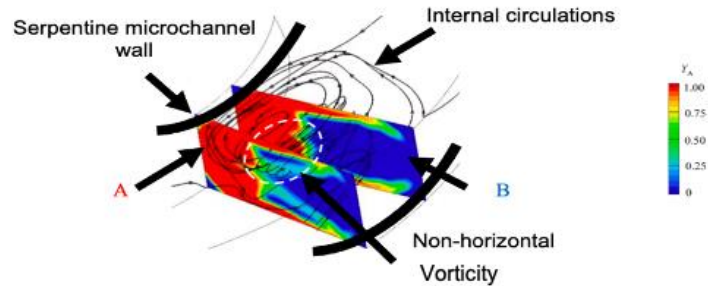
Figure 2 Components mixing inside droplet flowing through the uniform serpentine microchannel [16].

Chapter 3: Research Objectives

3.1 Problem Statement and Potential Benefits

In this project, a numerical investigation is performed using the Volume of Fluid method (VOF) to simulate several serpentine microchannels with a slug-based flow as a potential reactor for biodiesel production intensification to enhance the mixing for biodiesel production. Due to the dean forces at the curvature of the serpentine microchannel, some circular flows perpendicular to the fluid flow direction will be created which can enable the serpentine microchannel to induce secondary vortices next to the primary internal circulations [12]. This can consequently help to improve the mixing in the dispersed phase and increase the biodiesel production intensification yield at the interface compared to the conventional batch stirrer or straight microchannel. In this manner the mass transfer time can be optimized as well as the throughput of the biodiesel process. The slug flow pattern is chosen because of its high area-to-volume ratio which can increase the interfacial area between the reactants. The impact of both the geometrical dimensions (i.e., Curvature radius, width & corner shape) and operational parameters (i.e., alcohol to oil ratio) will be examined to optimize the microchannel mixing performance.

3.2 Research Challenges

The challenges associated with slug-based microchannels are predominantly rooted in the characteristics of microfluidic flows. These challenges are influenced by the laminar nature of flow in microfluidic channels and the difficulty of managing immiscible phases. In microfluidic channels, flows are typically laminar; hence, low limited mixing capabilities do occur due to the absence of turbulence, which hinders the introduction of vigorous mixing techniques. Achieving efficient mixing between immiscible phases in a laminar flow environment can be challenging, especially when compared to turbulent flows in larger-scale systems. Additionally, Slug flow patterns in microchannels are susceptible to multiple factors. One of the primary factors is the flow rate ratio between the immiscible fluids. The slightest changes in flow rates can result in shifts from slug flow to other flow patterns, such as annular or stratified flow. The flow rate ratio does not solely dictate slug flow behavior. Numerous parameters come into play, including fluid properties (e.g., viscosity, density), operational parameters (e.g., pressure, temperature), and geometry configurations of the microchannel (e.g., channel dimensions). The interplay of these factors makes slug formation a complex process. Addressing these challenges needs a comprehensive understanding of fluid dynamics, microchannel design, and the precise control of flow parameters.

3.3 Desirable Outcomes and Deliverables

This research aims to study the slug flow pattern hydrodynamics numerically in a serpentine microchannel as a potential reactor for process production intensification of biodiesel production. Through this study, the following objectives are targeted:

1- Study numerically the impact of changing geometrical dimensions, which are the microchannel curvature radius, channel width, and corner shape on vorticity, and analyze the reasons behind this impact.

2- Study numerically the impact of Alcohol to oil molar ratio changes on the slug size and vorticity.

3- Model a straight microchannel numerically and compare its performance to the performance of the serpentine microchannel.

Chapter 4: Methodology

4.1 Modeling

To perform the study, three different serpentine microchannels were simulated, in addition to one straight microchannel, using Ansys Fluent [17], which was deployed to study and illustrate the slug-based flow hydrodynamics with 2D mathematical modeling that consists of momentum conservation and interface-tracking models. The assumption of 2D simulation was made because the microchannel height impact is not part of the project scope. The energy balance model will be neglected since the system simulations were conducted under isothermal conditions at a temperature of 25 °C. The reaction was overlooked as the primary focus is on the hydrodynamic aspect. The adopted multi-component system was simulated with a laminar and non-compressible flow and transient condition. The interface-tracking technique is the volume-of-fluid (VOF) method [18] applied to obtain robust solutions for capturing the interface.

For model validation, a straight microchannel was simulated based on an existing literature [10], from which the experimental/operational parameters were extracted. The straight microchannel performance was then used for comparison against the serpentine microchannels.

A mesh test was conducted to validate the work and to find the best element size that generates similar results to the experimental results. The best element size was decided based on the slug length closest to the actual experimental slug length.

4.1.1 Volume of Fraction (VOF) Model

As mentioned previously, the governing equations consist of the Volume of Fraction (VOF) model [18] that represents the different species volume fraction inside a computational cell; F represents the phase fraction in the cell. Therefore, when F equals 1, it means that the cell is filled with palm oil (the continuous phase); when F equals 0, it means the cell is filled with methanol (the dispersed phase). F represents the transition region when it is equal to intermediate values between 0 and 1.

$$\frac{\partial F}{\partial t} + \nabla(F\vec{v}) = 0 \qquad (1)$$

Where, F is the volume fraction and $\vec{v}$ is the velocity vector of the mixture.

4.1.2 Equation of Continuity and Momentum Conservation Model

The equation of continuity and conservation of momentum model is presented as follows:

$$\nabla(\rho\vec{v}) = 0 \ (2) \ and, \quad \rho \cdot (\vec{v} \times \nabla\vec{v}) = -\nabla p + \mu\nabla^2 \cdot \vec{v} + \rho\vec{g} + \vec{F}_{sv} \ (3)$$

Where, ρ is the average specific mass and μ is the average dynamic viscosity of the mixture. While p is the pressure, $\vec{g}$ is the gravity acceleration which is equal to 0 since gravity is negligible at microscale and $\vec{F}_{sv}$ is the surface tension force.

14

4.1.3 Average Density and Viscosity Equations

In a two-phase system, the density and viscosity in each computational cell are calculated by the following equations considering both phases, the continuous and dispersed phases:

$$\rho = F_{PO}\rho_{PO} + F_M\rho_M \qquad (4)$$

$$\rho = F_{PO}\mu_{PO} + F_M\mu_M \qquad (5)$$

Where F_{PO}, F_M, ρ_{PO}, ρ_M, μ_{PO} and μ_M are palm oil phase volume fraction, Methanol phase volume fraction, palm oil density, methanol density, palm oil dynamic viscosity and methanol dynamic viscosity, respectively.

4.1.4 Surface Tension Force Equation

Surface tension force equation is described in equation 5:

$$\vec{F}_{sv} = \sigma \frac{\rho k \frac{n}{|n|}}{\left(\frac{1}{2}\right)(\rho_{PO} + \rho_M)} \qquad (6)$$

$$k = \nabla \frac{n}{|n|} \qquad (7)$$

Where σ and k are the surface tension and the local surface curvature. The local surface curvature is defined in terms of the divergence of the normal $\frac{n}{|n|}$.

4.1.5   Vorticity Equation

To calculate the vorticity which describes the rotation of fluid particles within a fluid flow, a mathematical expression was added to the simulation interface. The equation of vorticity is:

$$\omega = \frac{dv_y}{dy} - \frac{dv_x}{dx} \quad (8)$$

Where ω, dv_y and dv_y are vorticity, change of velocity in respect to y-axis and x-axis respectively.

High and low vorticity signifies the strength and intensity of the rotational or spinning motion exhibited by fluid particles in a specific location within a fluid flow. The most associated concept of vorticity is turbulence. Turbulence arises from the existence of vortices, swirls, and eddies in a fluid flow. These turbulence structures can enhance mixing by continually transporting fluid from different locations, thereby promoting the diffusion of reactants unless excessive turbulence occurs, resulting in ineffective mixing.

4.1.6　Boundary Conditions

Two alcohol-to-oil molar ratios are simulated for all the microchannels 7.6 and 22.9, which are within the molar ratio range discussed by the literature review of biodiesel production in microfluidic platforms [4]. The stoichiometric ratio of biodiesel production reaction is 3 but excess alcohol is always required to have a complete reaction (non-reversible). As per the literature review, the typical molar ratio is in the range of 6:1 to 12:1 (methanol to oil). Therefore, a molar ratio of 7.6 was chosen. For the 22.9 molar ratio, the main reason behind this selection is to see how the change in the volume fraction ratio between alcohol and triglyceride (from 0.33 (MR: 7.6) to 1(MR: 22.9)) will impact the slug size and vorticity. The boundary conditions for the two molar ratios are listed as following:

4.1.6.1 Alcohol to Oil Molar Ratio = 7.6

- No slip condition at the solid walls.
- At inlet 1, where the palm oil (Phase 1) is injected, the respective volume fraction and inlet velocity will be $F = 1$ and $v = v_{PO} = 0.669 \times 10^{-2} m/s$, respectively. The inlet velocity for the other component is $v_M = 0\ m/s$.
- At inlet 2, where the methanol (Phase 2) is injected, the respective volume fraction and inlet velocity are $F = 0$ and $v = v_M = 0.223 \times 10^{-2}\ m/s$, respectively. The inlet velocity for the palm oil is $v_{PO} = 0\ m/s$.
- At the outlet the gauge pressure is set to be zero.
- The contact angle of 135 degrees to account for the wall wettability.

Same as the previous case except for the following boundary condition:

- At inlet 1, where the methanol is injected, the respective volume fraction and inlet
  velocity are equal to F = 0 and $v = v_M = 0.446 \times 10^{-2}\ m/s$, respectively. The inlet
  velocity for the palm oil is equal to $v_{PO} = 0\ m/s$.

- At inlet 2, where the palm oil is injected, the respective volume fraction and inlet velocity
  will be equal $F = 1$ and $v = v_{PO} = 0.446 \times 10^{-2}\ m/s$, respectively. The inlet velocity
  for the other component is equal to $v_M = 0\ m/s$.

Table 1 Boundary Conditions Summary

Molar ratio	7.6		22.9	
Reactant	Palm oil	Methanol	Palm oil	Methanol
Inlet 1	$F = 1$ $v = v_{PO} = 0.669 \times 10^{-2}\ m/s$	$v_M = 0$	$F = 1$ $v = v_{PO} = 0.446 \times 10^{-2}\ m/s$	$v_M = 0$
Inlet 2	$v_{PO} = 0$	$F = 0$ $v = v_M = 0.223 \times 10^{-2}\ m/s$	$v_{PO} = 0$	$F = 0$ $v = v_M = 0.446 \times 10^{-2}\ m/s$
Outlet	Pressure gauge = 0			
Wall	No slip condition			
Contact angle	135°			

4.2 Reactants: Methanol and Palm Oil

The reactants used for the simulation are palm oil and methanol. The physical properties, such as

density, viscosity, and surface tension of palm oil and methanol, are shown in table 1 [10].

Methanol is recognized for its cost-effectiveness and favorable physical and chemical advantages. For instance, when used in biodiesel production, methanol yields biodiesel with reduced viscosities compared to ethanol. Additionally, palm oil is distinguished mainly for its very high cetane number due to the presence of saturated fatty acids like palmitic acid and stearic acid, which means it is easy to combust when used as a fuel [19].

Table 2 Physical Properties of Palm Oil & Methanol at 25 ºC [10]

Property	Density (kg/m^3)	Viscosity $(Pa.s)$	Surface tension (N/m)
Palm oil	909	69.1×10^{-3}	3.27×10^{-3}
Methanol	785	0.55×10^{-3}	

4.3 Geometry Dimensions

To explore the best potential geometry configuration, the internal wall corners, and curvature radius will be varied. The internal wall corners will be either 90-degree or rounded corners (corner diameter is 400 µm). The external wall corners will not be varied since there is no contact between the slug and the external wall due to centrifugal forces. The curvature radius is also studied by changing the length of the longer segment of the serpentine microchannel unit to study their effect on vorticity. The lengths that are compared are 2000 µm and 1000 µm.
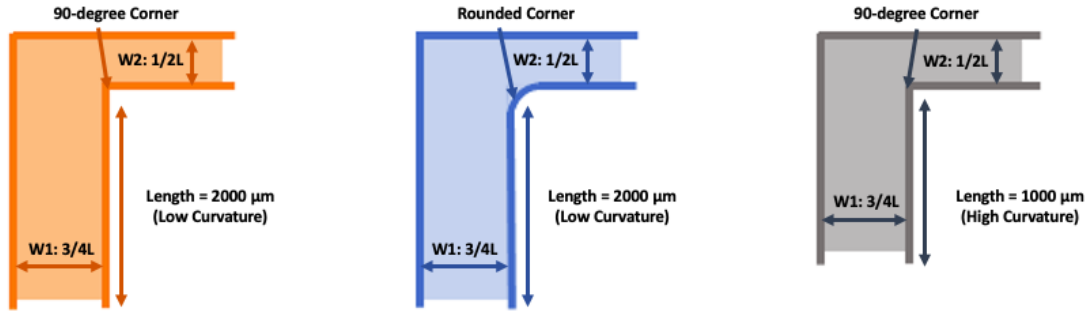
Figure 3 Geometry Dimensions Variations in The Serpentine Microchannels

Moreover, all the serpentine microchannels discussed in this project have a changing width as depicted in Figure 3. Based on the Dean Number equation (8), employing a serpentine with changing width (i.e., diameter) has a higher Dean Number than the one with a constant width which means it should have stronger vorticities along the channel. The reason behind this is that the velocity increased with the smaller width which increased the Reynolds Number and the Dean Number accordingly [20]. The Dean Number analysis of both varying and constant widths is shown in Table 3. Detailed calculations of Dean Number are attached in Appendix B.

$$De = \frac{\rho v D}{\mu} \left(\frac{D}{R}\right)^{0.5} \quad (9)$$
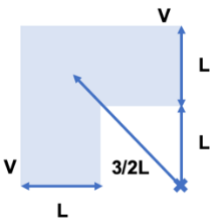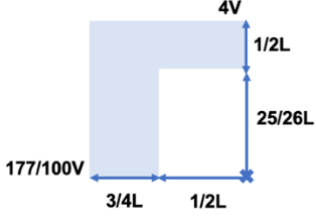
Where, De, D, and R are Dean Number, diameter, and curvature radius respectively [21].

Four microchannel configurations that have been studied, considering the varying geometrical features mentioned above, are listed below:

1. Straight Microchannel

2. Serpentine Microchannel with 90-degree Corners with low curvature

3. Serpentine Microchannel with Rounded Corners with low curvature

4. Serpentine Microchannel with 90-degree corners with high curvature

The dimensions of the microchannels are illustrated in Table 4. Important note to make is that all microchannels have the same inlet dimensions.

Table 3 Dean Number Analysis [21]

Serpentine Microchannel Type	Serpentine Microchannel with Constant Width	Serpentine Microchannel with Varying Width
Schematic		
D	$= L$	$= \dfrac{\left(\dfrac{3L}{4} + \dfrac{L}{2}\right)}{2} = \dfrac{5L}{8}$

R	$= \dfrac{3L}{2}$	$= \dfrac{\left(\dfrac{17L}{10} + \dfrac{107L}{100}\right)}{2} = \dfrac{277L}{200}$
R_e	$= \dfrac{\rho \cdot v \cdot L}{\mu}$	$= \dfrac{\rho \cdot \dfrac{72}{25} v \cdot \dfrac{5}{8} L}{\mu}$
$\sqrt{\dfrac{D}{R}}$	$= \sqrt{\dfrac{1L}{1.5L}} = 0.82$	$= \sqrt{\dfrac{0.625L}{1.385L}} = 0.672$
D_e	$= 0.82 \cdot \dfrac{\rho \cdot v \cdot L}{\mu}$	$= 0.672 \cdot \dfrac{\rho \cdot \dfrac{72v}{25} \cdot \dfrac{5L}{8}}{\mu}$ $= 1.2 \cdot \dfrac{\rho \cdot v \cdot L}{\mu}$

Table 4 Microchannels Configurations and Geometry

Configuration Geometry	Configuration Description
	Straight Microchannel
	Serpentine Microchannel with 90-Degree Corners & Low Curvature
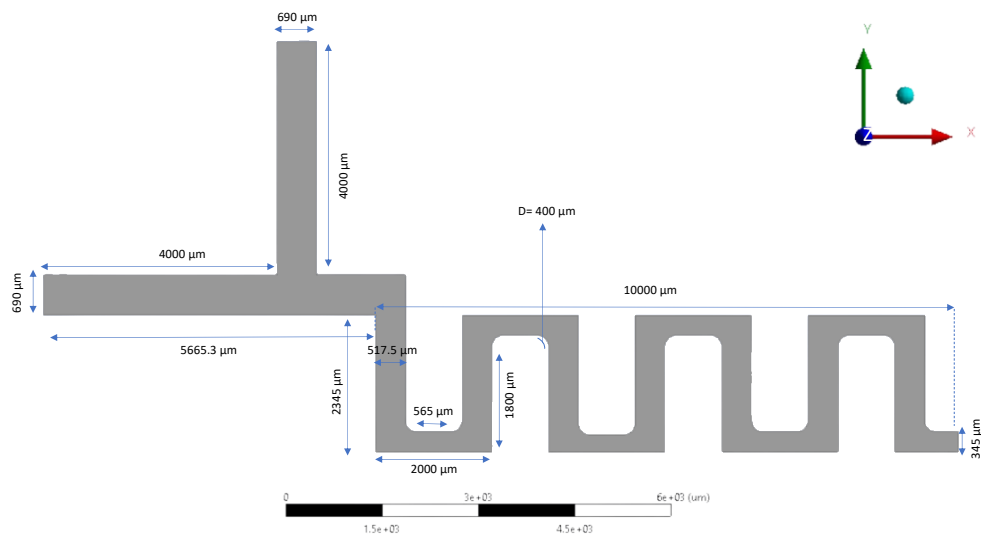
Serpentine Microchannel with Rounded Corners & Low Curvature

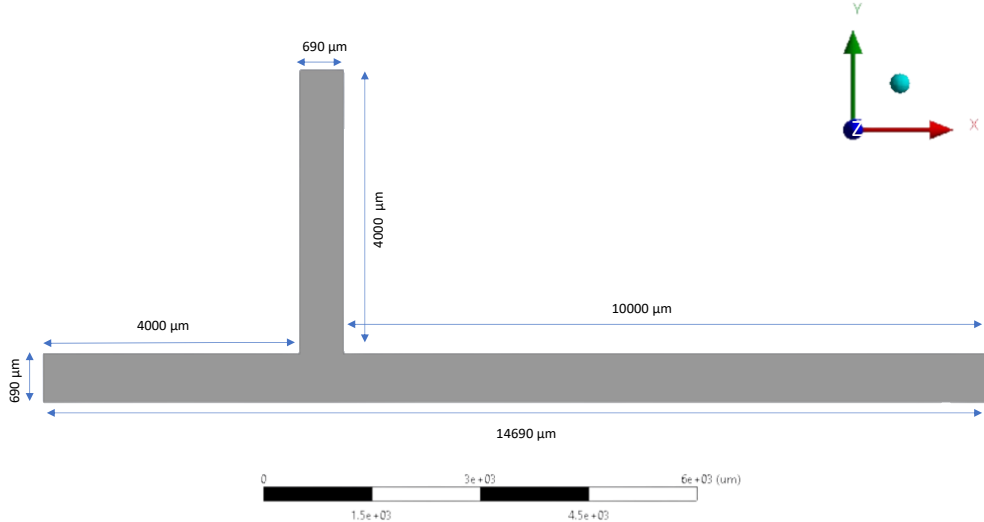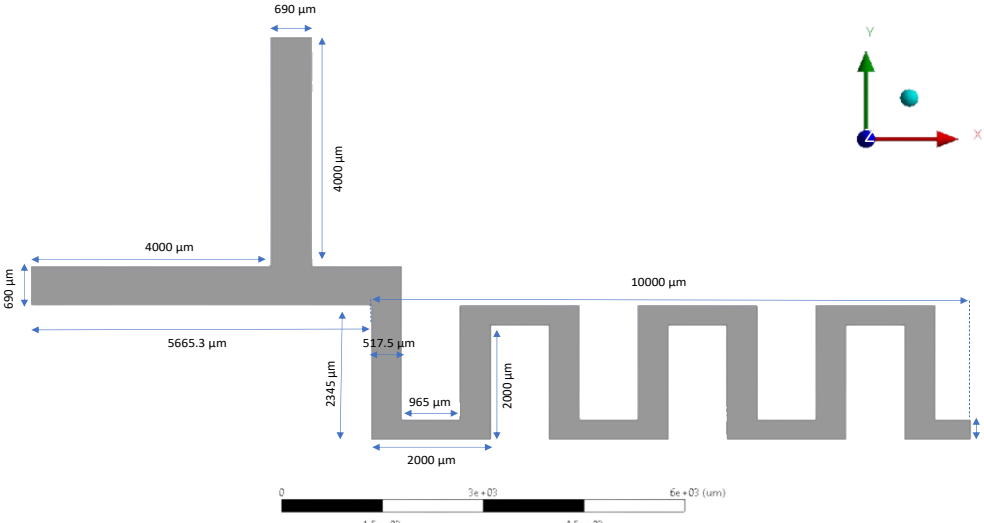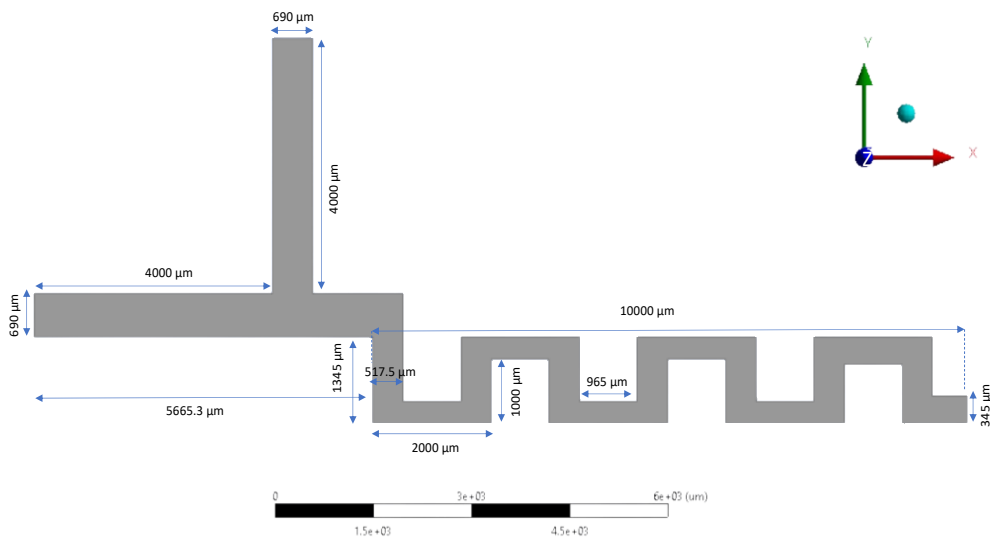Serpentine Microchannel with 90-Degree Corners & High Curvature

4.4 Operational Parameters

All the operational parameters will be kept constant except for the molar ratios and the corresponding velocities. The total volumetric rate and temperature are set to be 200μL/min and 25℃ respectively. The catalyst concentration is omitted as it has no influence on the hydrodynamics of the multiphase system [10], and the reaction is not considered within this study. However, it is important to understand that for all operational parameters, the optimal values could be different from system to system depending on the utilized reactants and mixer.

4.5 Modeling Outputs

The impact of the variation of the mentioned parameters will be illustrated in terms of volume fraction profile, circulation streamlines, vorticity contour, and vorticity to evaluate the hydrodynamics and mixing performance in all the microchannels configurations.

4.6 Validation and Comparison

The slug length from the simulation results in the straight microchannel is compared with the existing experiment from [10] at the operational parameters of a molar ratio of 7.6 at 25℃ & 200μL/min to validate the model simulation. After validation, to study the mixing enhancement made by the serpentine microchannels, the serpentine microchannels simulation results will be compared to the straight microchannel with a slug flow pattern under the same conditions.

Chapter 5: Results and Discussion

5.1 Mesh Test and Validation

To validate the models, the slug length from the experimental work of [10] was compared to the simulation slug length generated for this project at a molar ratio of 7.6 in a straight microchannel. The slug length was simulated at different mesh cell sizes as shown in Table 5 below. The experiment slug length in [10] was measured to be 717.00 µm. The mesh element size that was selected is 20µm with a slug length deviation of 4.60%. Hence, a mesh cell size of 20 µm was utilized for the rest of the study.

Table 5 Quantitative analysis of the comparison between simulation and experimental results at different meshing qualities

Mesh Cell Size (µm)	Slug Length (µm)	Number of Element	Deviation (%)
30	751.10	19168	4.76
25	749.99	26755	4.60
20	749.99	39931	4.60
15	749.34	67051	4.51

5.1 Hydrodynamics study

5.2.1 Case 1: Alcohol to Oil Molar Ratio = 7.6

5.2.1.1 Volume of Fluid Profile

Straight Microchannel

As per the volume fraction profile in Figure 4, the straight channel is initially full of palm oil, which is the continuous phase. At t=0, the methanol enters the inlet and forms a rounded interface once it is in contact with the palm oil phase. The methanol continues traveling along the inlet until it reaches the main channel. At this point, the methanol slug will start to form, and then it will break off due to the pressure build-up in the continuous phase [22]. Once the methanol slug is entirely detached from the neck due to the domination of the interfacial forces [23], other slugs along the channel will follow as time proceeds.

It was observed that there is a thin film of palm oil between the wall and the slug interface due to the wall's high hydrophobicity, as a result of assigning a contact angle of 135º at the walls of the channels [23]. In addition to the hydrophobicity, the Capillary Number plays a massive role in forming such thin films. The capillary number is defined as the product of dispersed phase (i.e. methanol) velocity and continuous phase (i.e. palm oil) viscosity divided by the surface tension which resembles the ratio of the viscous forces to interfacial forces as shown in equation 9, where, Ca is the Capillary Number. In this study the capillary number of the straight microchannel was found to be 0.04 and as stated by Raimondi et. al (2008), when the Capillary Number is higher than 0.01, a thin film of the continuous phase always exists between the dispersed phase slugs and the straight microchannel wall [24]. The Capillary number for the flow in the straight channel was 0.04, which guarantees the existence of this thin film. Moreover, it was perceived that the slug is

formed in the shape of a bullet where it has a flat rear and more like a rounded front. The bullet

shape of the slug is characterized by the Capillary number that is higher than 0.02 [25,26,27]. The

slug keeps its shape until it reaches the channel's end at t= 2.452s.
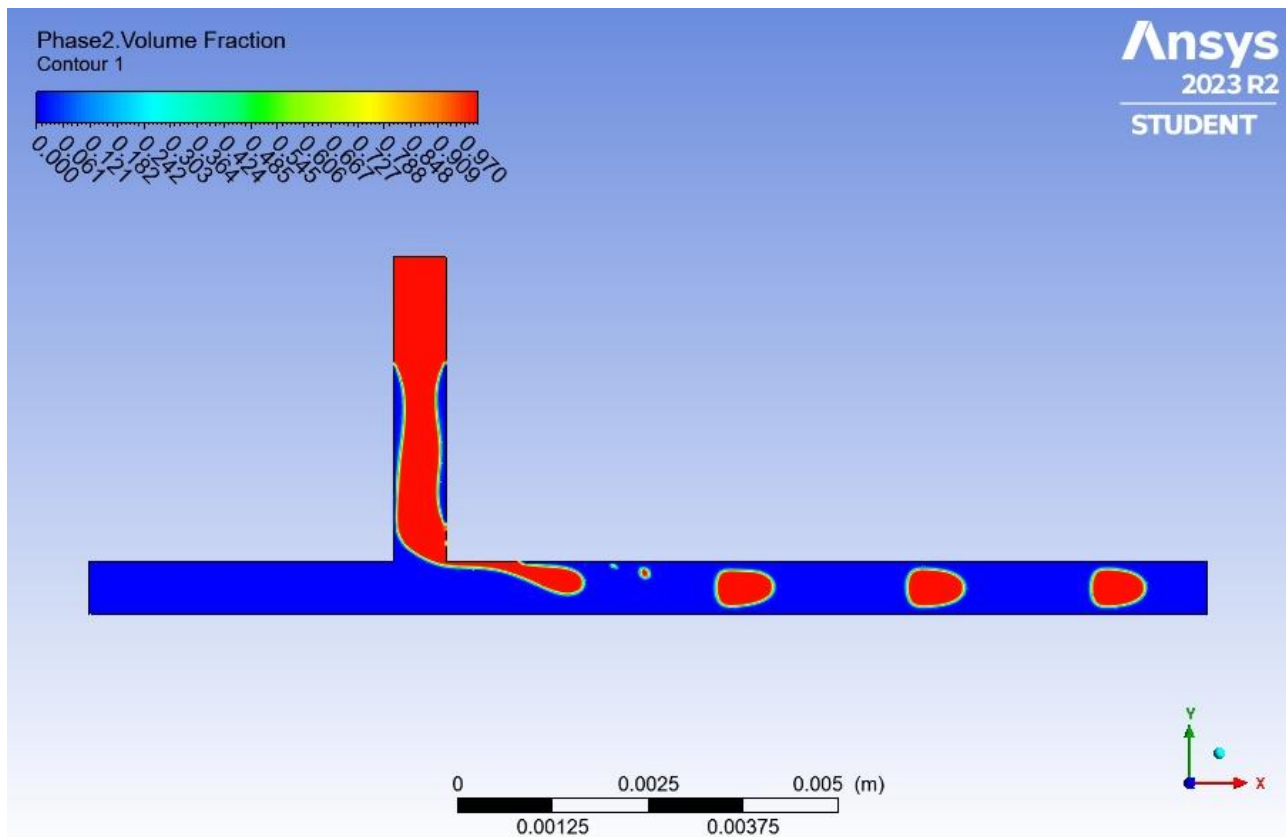
$$Ca = \frac{v_M \cdot \mu_{PO}}{\sigma} \quad (10)$$

Figure 4 Straight Microchannel VOF Profile for Molar Ratio of 7.6 (Note: the black and white scale bar signifies the dimension of the geometry)

The VOF profile of the serpentine microchannel with 90-degree corners and low curvature is shown in Figure 5. When the slug moves along the 517.5 µm width segment (point 1), it can be observed that this time, the slug is more elongated because the width here is smaller than the inlet channel width (ID= 690 µm). Moreover, when the slug enters the 345 µm width segment (point 2), the slug will be even more elongated at this point due to the smaller width than the previous segment (point 1). Moreover, it can be observed that the slug is always moving next to the internal wall instead of the external. Also, as the slug moves along the channel, the corners impact the shape of the slug from both sides. When the slug travels in the left-hand side (LHS) units of the microchannel, only the right side of the slug will be exposed to the sharp 90-degree corners, but when the slug moves in the right-hand unit (RHS) of the microchannel, the left half of the slug will be exposed to the 90-degree corners. The slug reaches the end of the channel at t= 2.907s.
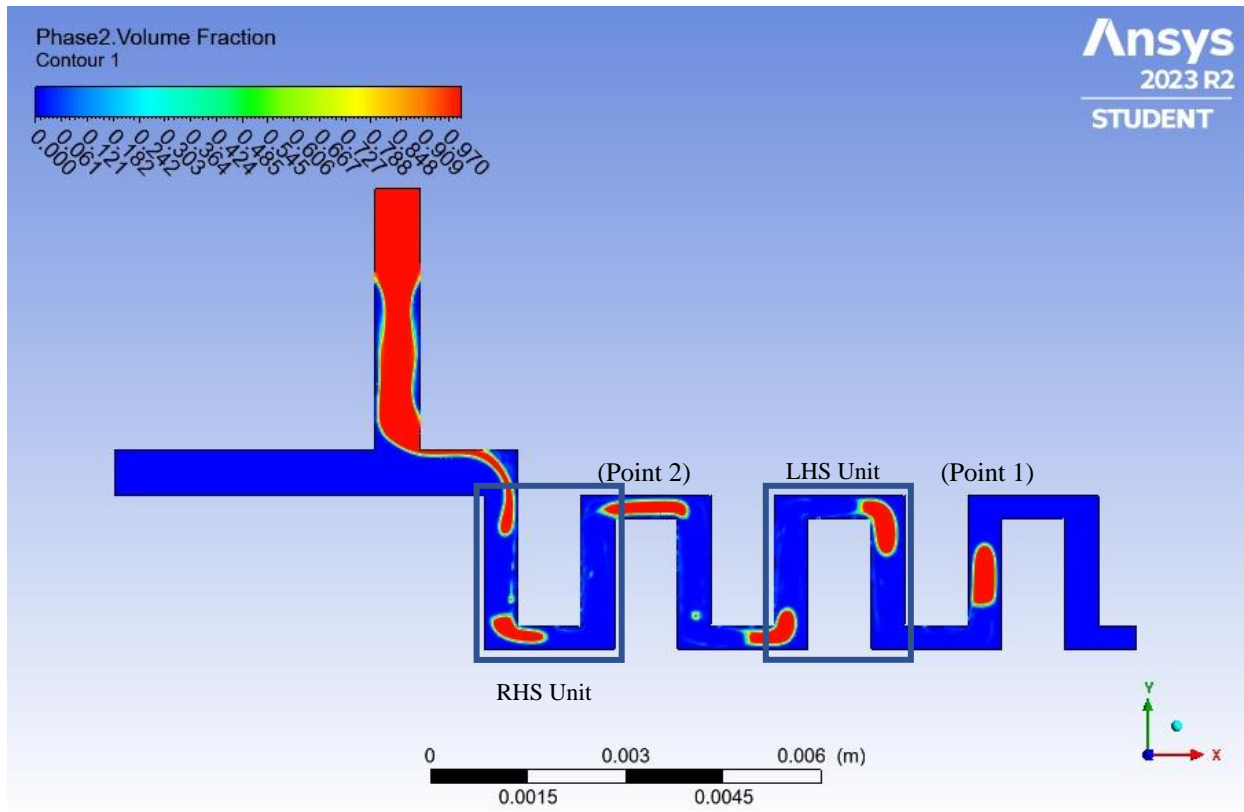
Figure 5 Serpentine Microchannel with 90-Degree Corners and Low Curvature VOF Profile for Molar Ratio of 7.6 at Different Locations

Serpentine microchannel with rounded corners and low curvature

In the rounded corners microchannel, as illustrated in Figure 6, the movement of the slug along the channel is the same as the previous serpentine microchannel, except for the corners. It was observed that the 90-degree corners squeezed the slug compared to the rounded corners, decreasing the area in the corners compared to the rounded corners. Consequently, the average slug length around the 90-degree increased compared to the rounded corners, which are measured to be 1399μm and 1275μm, respectively. The slug reaches the end of the channel at t= 2.904s.
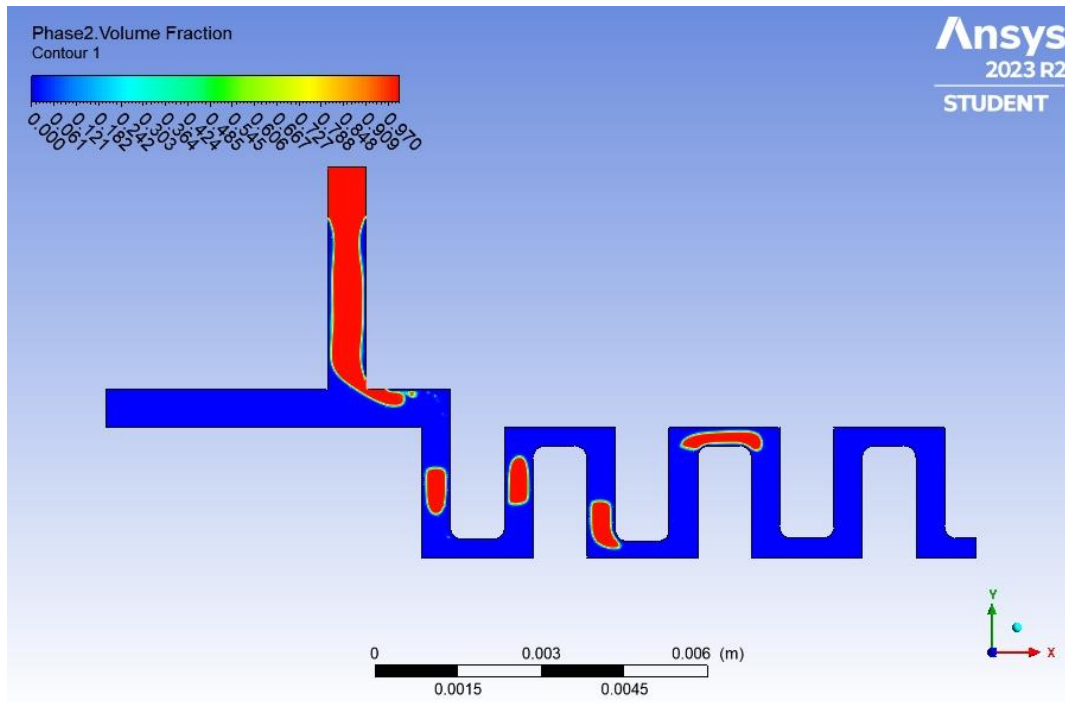
Figure 6   Serpentine Microchannel with Rounded Corners and Low Curvature VOF Profile for Molar Ratio of 7.6

Serpentine Microchannel with 90-degree Corner and high curvature

In the high curvature microchannel, it can be observed that the slug will spend less time on the 517.5µm width segment (point 1) than the two previous serpentine microchannels because the length of this segment is reduced from 2000 µm to 1000 µm. Moreover, it can be noticed that the slug flowing in the point 1, has its two ends around the corners due to the shorter length of the segment. The slug reaches the end of the channel at t= 2.485s
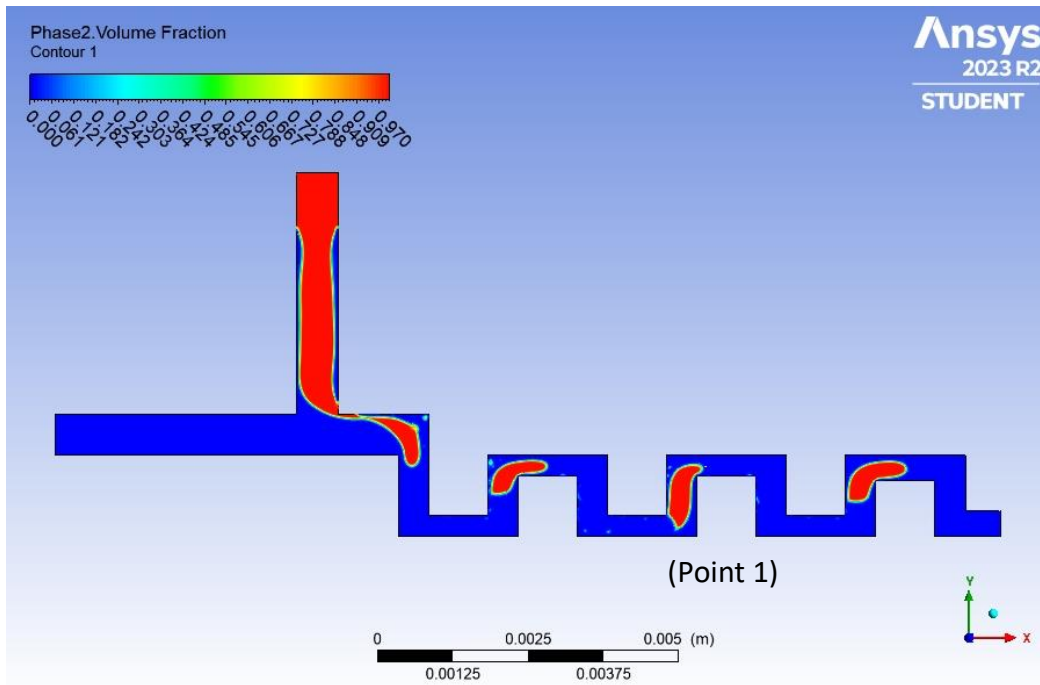
Figure 7 Serpentine Microchannel with 90-degree Corner and High Curvature VOF Profile for Molar Ratio of 7.6

5.2.1.2 Internal Circulation Streamlines

Straight Microchannel

The internal circulation in a slug flow traveling in a straight microchannel is illustrated in Figure 8, showing that the slug contains several internal circulations, as expected for flows with low Capillary and Reynolds Number [24]. Two of the total six circulations are considered the major circulations which are in the center of the slug, located at the left and right halves of the slug. The other four circulations which are smaller in size are the minor circulations and are located at the front and the rear of the slug, on both sides, the left and the right as well. The major circulations are initiated due to the shear contact between the continuous phase around the slug and the walls.

In contrast, minor circulations arise from the interaction between the droplet and the bulk continuous phase. The major and minor circulations are distributed symmetrically along the axis of the straight microchannel. Additionally, several stagnant regions were identified in the slug, located at the left and right halves as well as at the front and rear, which is the same as reported in reference [28].
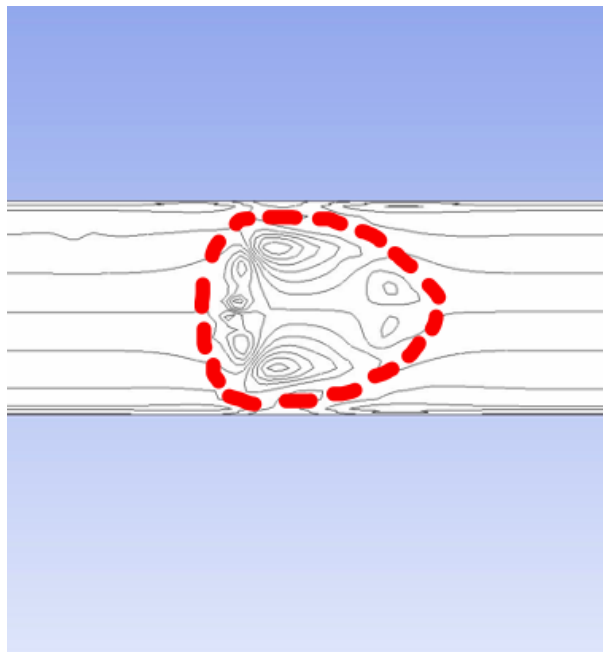

Figure 8 Internal Circulations in the Straight Microchannel for Molar ratio of 7.6

Serpentine Microchannel with 90-degree Corners and Low Curvature

In the 517.5 µm width segment (Figure 9A), the slug looks like a bullet with two major circulations and four minor circulations as it was observed with the straight microchannel but with more

congested circulation streamlines since the width here is smaller compared to the width of the straight microchannel which is 690 µm.

Around the 90-degree corner (Figure 9B) the slug, as well as the major and front minor circulations, start to deform. To clarify, the major circulations are broken into small ones formed in the middle of the slug (i.e., chaotic advection). The symmetry within the slug in the serpentine microchannel is no longer maintained due to the flow direction change due to the corners [29] and the stretching due to the cross-section variation. Both phenomena lead to an asymmetrical distribution of internal circulations.

Afterward, the slug gets more elongated as it enters the 345 µm width segment (Figure 9C), and the streamlines get even more congested. Also, it was observed that the minor circulations in the front of the slug start to lose their shape as the slug enters the 345 µm width segment further. When the whole slug is in the 345 µm width segment, it can be claimed that front circulations are completely deformed and vanish. Additionally, the major circulations started to form back. This indicates that the existence of the corners and the change in flow direction directly increases the chaotic advection, while the reduction of the width impacts the Dean vortices indirectly, through the increment in velocity as discussed in section 4.3.

Once the slug leaves the 345 µm width segment and it is completely in the 517.5 µm width segment (Figure 9E) both the major and minor circulations regain their shapes.

Figure 9 Internal Circulation in Serpentine Microchannel with 90-Degree Corners and Low Curvature for Molar ratio of 7.6 at Different Locations: (A&E) 517.5 μm width segment (B&D) Corners (C) 517.5 μm width segment (Note: The slug moves from location (A) to (E))

Serpentine Microchannel with Rounded Corners and Low Curvature

For the rounded corners serpentine, the slug looks and behaves exactly as the previous serpentine microchannel except around the corners. Around the rounded corners, the slug starts to deform as well as the slug circulations but this time without any intensive intrusion. With the rounded corner, major circulations are broken into fewer small circulations compared to the 90-degree corner.

Figure 10 Internal Circulations in Serpentine Microchannel with Rounded Corners and Low Curvature for Molar ratio of 7.6

Serpentine Microchannel with 90-degree Corners and High Curvature

With high curvature serpentine, the slug will be deforming continuously due to the short length of the 517.5 µm width segment. Once the slug rear leaves any of the segments, its front will enter the next quickly. As shown in figure 11, when the slug leaves the 345 µm width segment and enters the 517.5 µm segment in Figure 11A, its rear will be deforming and till the rear regains it is original shape in the 517.5 µm width segment, the front of the slug will enter the next 345 µm width segment (figure 11B) and it will be starting to minimize its front two circulations till they are entirely deformed.

Here, it can be claimed that the minor circulations do not have enough existence time in the channel. Once it is formed, it will be deformed again, which, in this case, means that the impact of the minor circulations in this microchannel will be less compared to the other configurations. On the other hand, the major circulations were also impacted by the shorter segment. Instead of having six symmetrical circulations, the circulations formed are broken and asymmetrical (figure 11A).
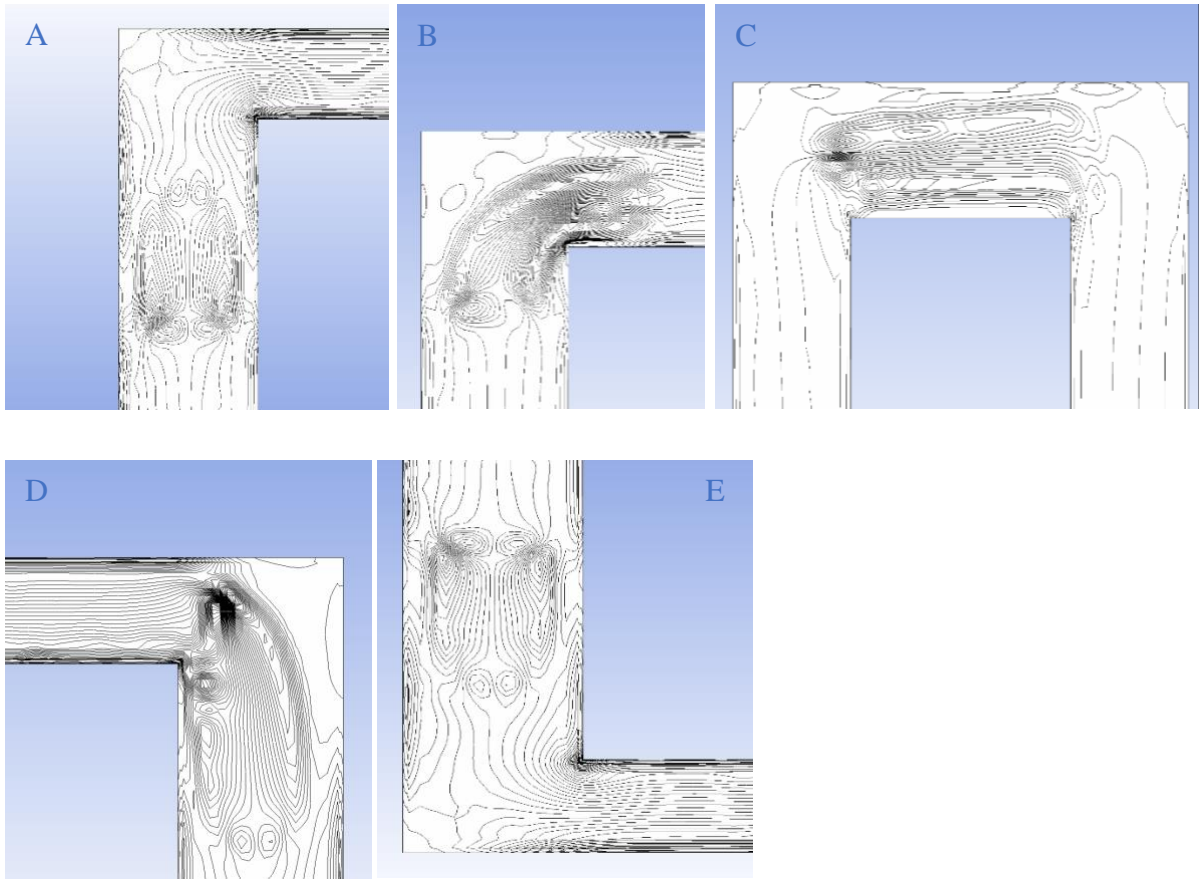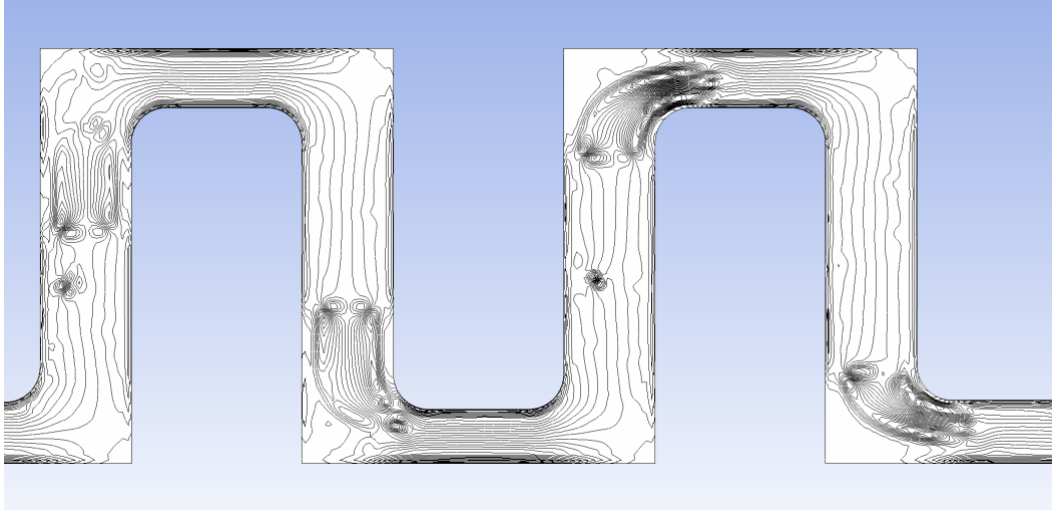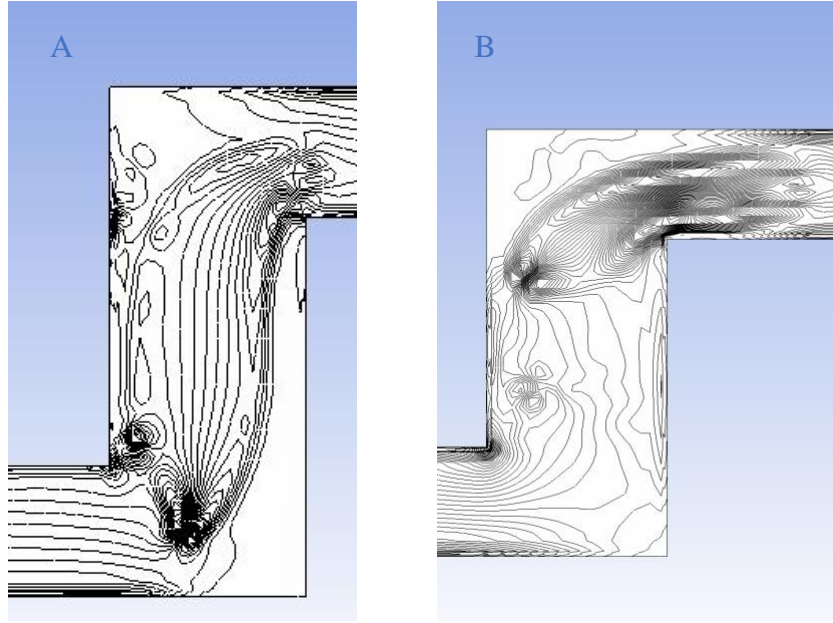
Figure 11 Internal Circulations in Serpentine Microchannel with 90-degree Corners and High Curvature for Molar ratio of 7.6 at Different Locations (A) 517.5 μm width segment & (B) Corner

With all the microchannel types, it was observed in Figures 12, 13, 14, and 15 that the two major circulations within the slug (slugs are outlined in red rectangles) move in opposite directions. The left half circulation moves counterclockwise, which means it travels forward to the front of the slug, then to the rear, and back again to the center of the slug. The same happens with the right half of the primary circulation but in a clockwise direction, moving back to the rear of the slug, then to the front, and then back again to the center of the slug. Per the vorticity profiles, the counterclockwise movement is denoted with positive vorticity values, and the clockwise movement is denoted with negative vorticity values [30,31].

Figure 12 Straight Microchannel Vortices Contour for 7.6 Molar Ratio

Figure 13 Serpentine Microchannel with 90-degree Corners and Low Curvature Vorticity Contour for Molar ratio of 7.6
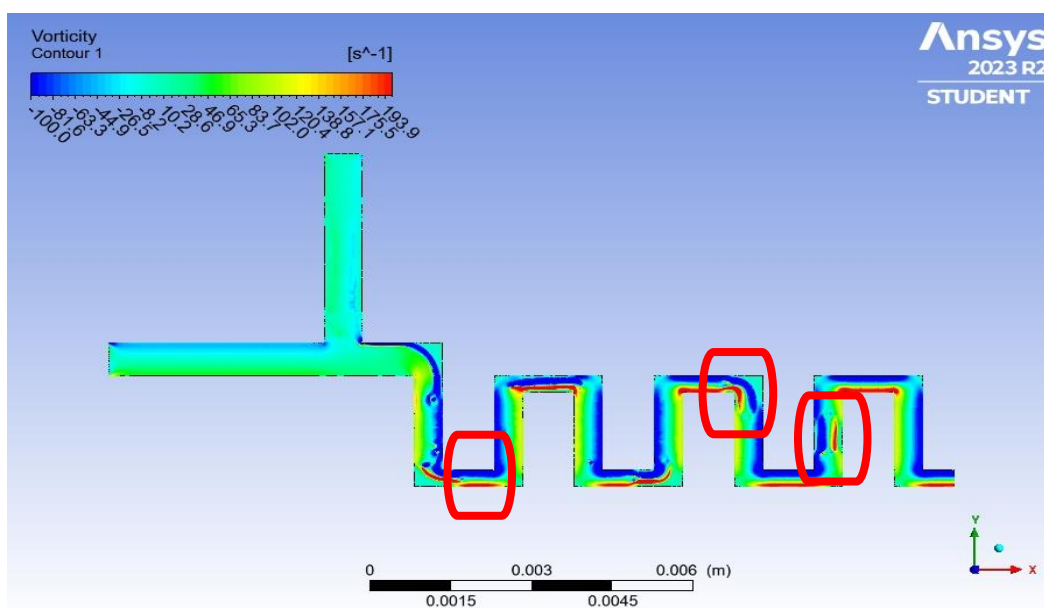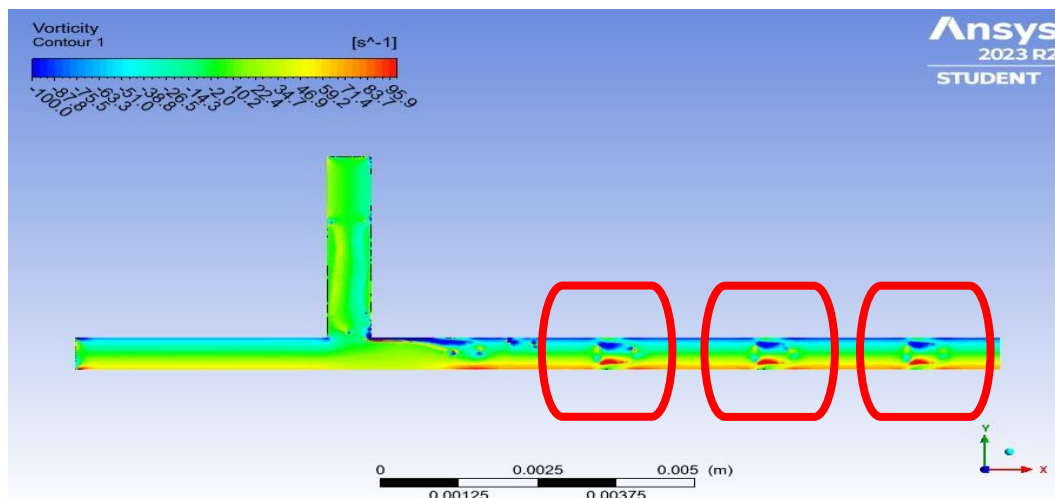
Figure 14 Serpentine Microchannel with Rounded Corners and Low Curvature Vorticity Contour for Molar ratio of 7.6

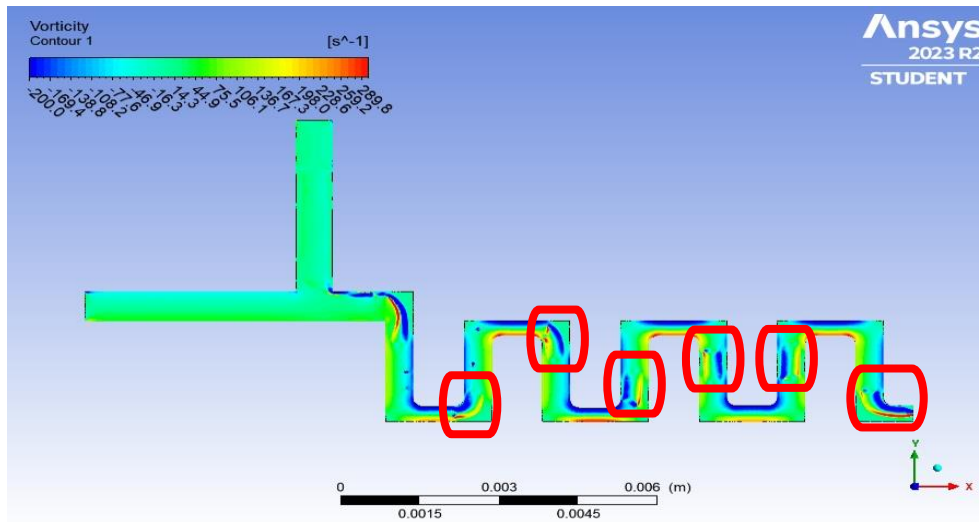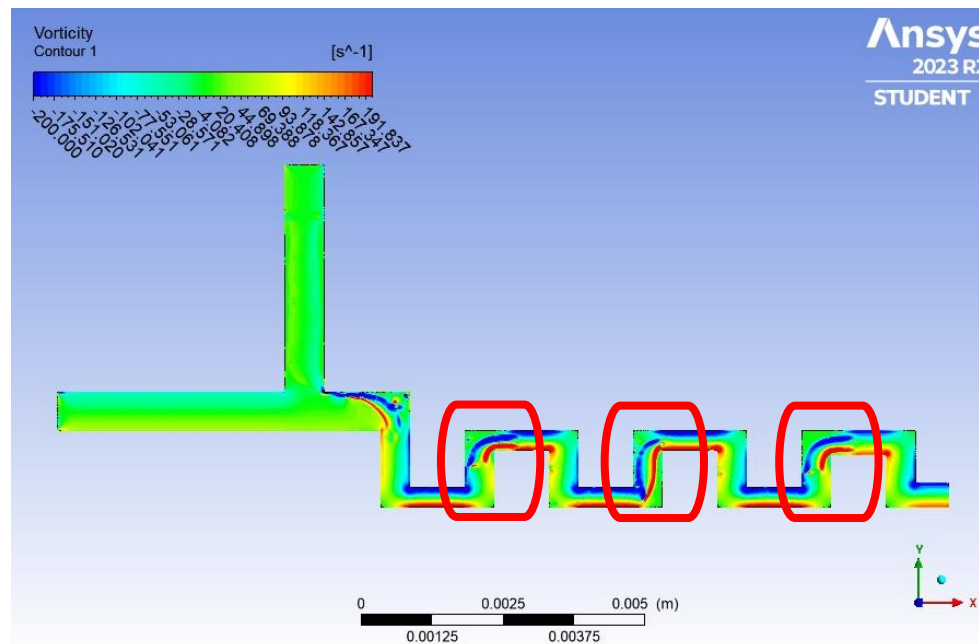*Figure 15 Serpentine Microchannel with 90-degree Corners and High Curvature Vorticity Contour for Molar ratio of 7.6*

5.2.1.3 Vorticity Measurement

Based on the slug vorticity profile for each serpentine microchannel and the straight microchannel, the major circulation vorticity was measured using a point function in Ansys Fluent. The measurements were taken at different locations along the main channel of the straight microchannel and along one single unit of a serpentine microchannel, as illustrated in Figure 16. This was done to study the impact of the width, corners, shape curvature radius and to compare the performance of both the straight microchannel and the different serpentine microchannel configurations.
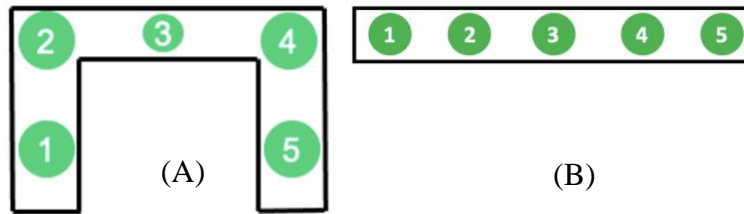
Figure 16 Vorticity Measurement Locations for Both A) Single Unit of Serpentine Microchannel and B) Straight microchannel

To study the impact of the width, the vorticity measurements in locations 1, 3 and 5 were compared. As depicted in Figure 17, the vorticity value was found highest in location 3 for all the serpentine microchannels associated with the smaller width, 345 µm. This was due to the velocity increment (with constant total volumetric flow rate) as width decreases, as per the Dean Number analysis in section 4.9. The velocity increment when width decreases enhanced the Reynolds number and, consequently, the Dean Number. The same trend was reported in [32], especially for

aspect ratios (i.e., channel width to channel height ratio) from 0.5 to 1.5 due to the increment in Dean Velocity. When it comes to mixing, increasing the channel width while keeping the other dimensions constant increases the mixing length since the liquid slug volume increases, which means that the mixed volume per mixing time decreases as the channel width increases [33,34]. In a separate investigation [35], the enhancement in internal circulation inside the slug and consequently mass transfer at the interface was achieved when the hydraulic diameter was reduced from 600μm to 400μm and it even increased further when reduced from 400μm to 200μm.

Figure 17 Width Impact on Vorticity (Location 1, 3 & 5)

Corners were investigated at locations 2 and 4 to check which corner shape resulted in higher vorticity. The results showed that the 90-degree corner induced slig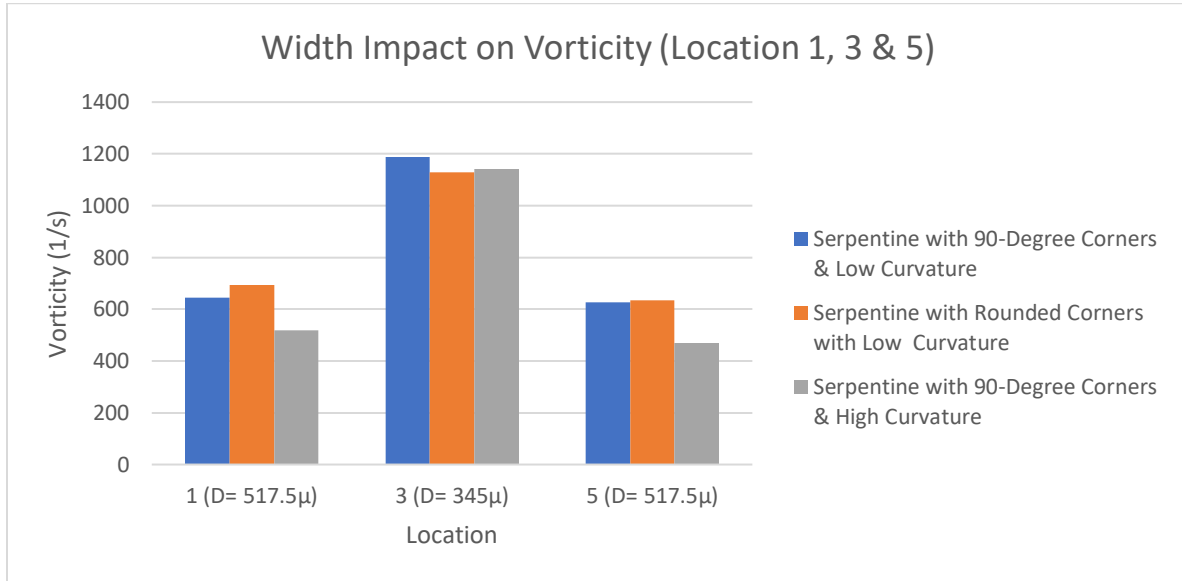htly higher vorticity than the rounded corner. This minor difference is due to the chaotic advection and broken internal

circulations found around the 90-degree corner per the Dean Vortices circulation profile discussed previously. When calculating the microchannels' Bend Ratio (i.e., ($\bar{R} = W/R_b$), where R_b is the bend radius) of the 90-degree and rounded corners, it was found that they equal 0 and 1.04, respectively. Similarly, in [36], they found that the 0 and 1 Bend Ratios resulted in similar mixing efficiency while the corner bends with the lower bend ratios resulted in lower mixing efficiency. As stated by Dean Number equation the higher the width to Radius ratio the stronger the vorticity.

Another point to mention is that the vorticity in location 4 was found to be less than that in location 2; this might be because the slug in location 2 is moving from a broader width to a narrower width while the slug in location 4 was moving from a narrower width to a wider width.
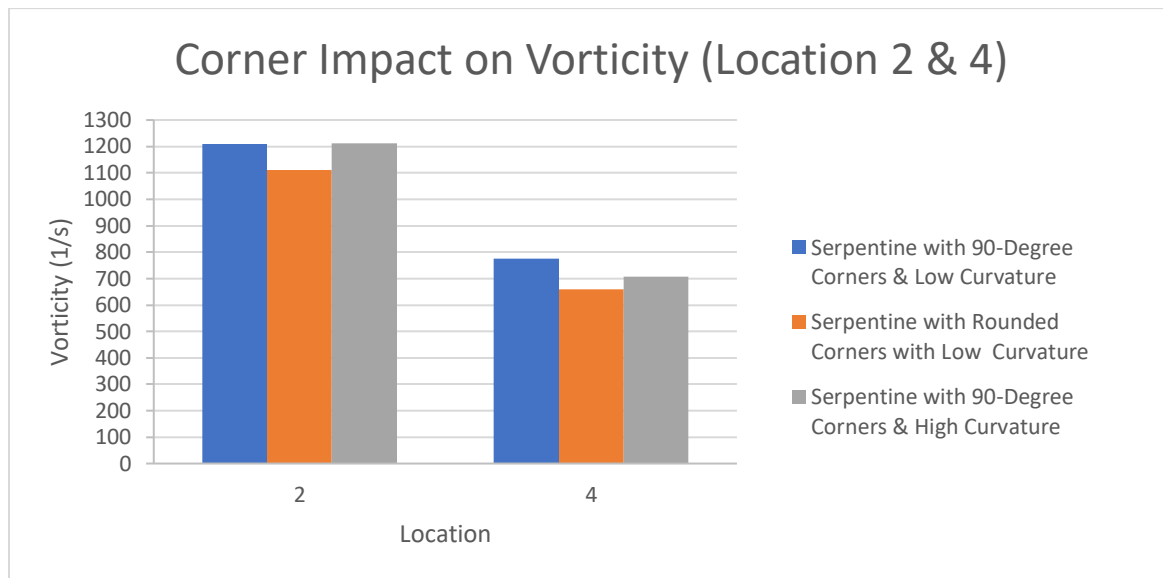

Figure 18 Corner Impact on Vorticity (Location 2 & 4)

To study the impact of the curvature on the vorticity, the vorticity measurements were taken at locations 1 and 5 for each serpentine microchannel. It was found that the serpentine with the low curvature (i.e., large radius) has higher vorticity compared to the high curvature, although the Dean

Number equation says the opposite. This might be due to the continuous and over-deformation that the high curvature (i.e., small radius) caused to the slug's internal circulations, which did not favor higher vorticity. For the mass transfer, occasionally, the longer radius is preferred because it gives enough mixing time and length for the fluids to mix [37].
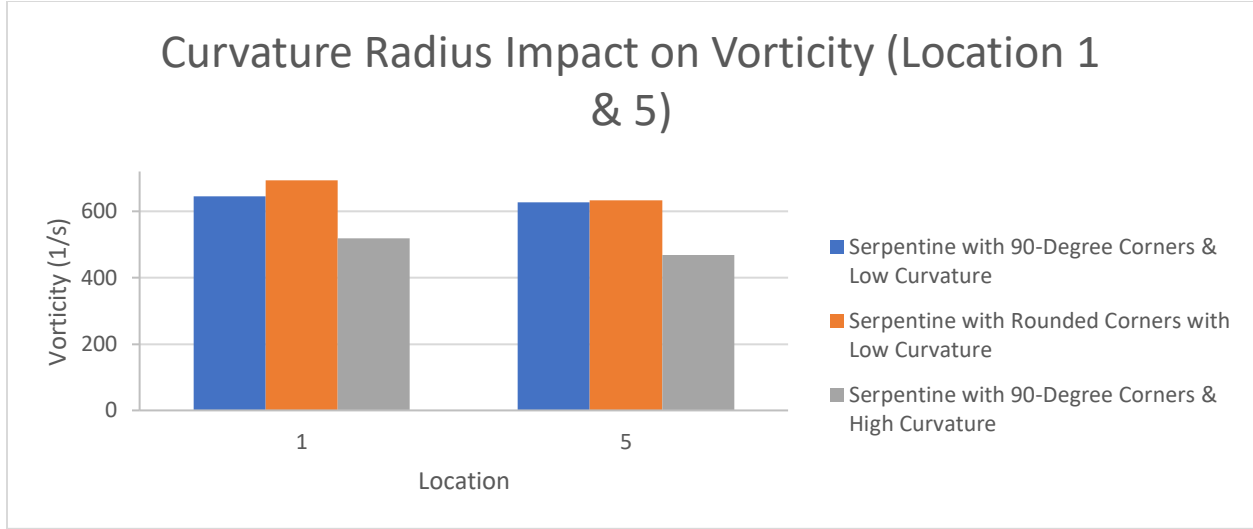
Figure 19 Curvature Impact on Vorticity (Location 1 & 5)

The vortices versus the location versus the microchannel configuration were plotted in Figure 20 to compare all the microchannel configurations. It was found that the straight microchannel induced the lowest vorticity. The vorticity in a straight microchannel was found to be almost the same in all the locations. The vorticity average in these locations is (ω=353.677 1/s). This is due to the bigger width and the absence of the bends, which lead to the lack of chaotic advection and asymmetrical circulations inside the slug. The symmetrical circulations will impact even the mass transfer inside the slug, hindering the concentration redistribution in the radial direction and allowing it only in the axial direction [38,39]. When it comes to the serpentine microchannels, the 90-degree corner microchannel with the low curvature induced the highest vorticity (ω=888.872

1/s), followed by the rounded corner microchannel with the low curvature (ω=845.041 1/s) and then the 90-degree corner microchannel with the high curvature (ω=809.506 1/s). When comparing the 90-degree corner microchannel with the low curvature to the other serpentine microchannels, it was found that the curvature radius has a more significant impact on the vorticity than the corner shape; this might be due to the close Bend Ratios of the 90-degree and the rounded corners. The impact of the serpentine microchannel on mixing efficiency is due to the role of secondary vortices stretching and folding in increasing the interfacial area, which can increase the mixing performance from 1.6 to 16 times compared with a straight microchannel [39,40].

Referring to Tung et al. (2009), who studied a similar system to this study - especially the geometry of the microchannels - it was found that the mixing index increased by 533% when the vorticity improved by 134.7% [21]. In our system, the vorticity increased by 232.996%, so it is anticipated that the mixing index will be enhanced by 900% or above (if the relationship between vorticity and mixing is assumed to be linear). The main differences between the [21] study and this study are the fluids (water and oil) used, the velocity of the fluids (which is less than this study), and the dean number, which is less than our study by 16.6%.
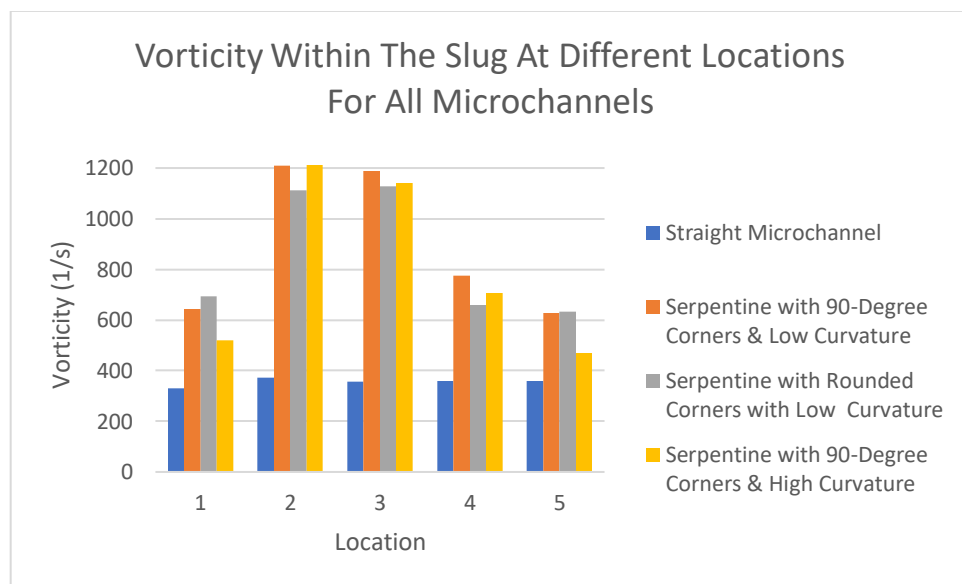

Figure 20 Vorticity within the Slug at Different Locations for All Microchannel Configurations

44

5.2.2 Case 2: Alcohol to Oil Molar Ratio = 22.9

5.2.2.1 Volume of Fraction Profile

Straight Microchannel

As per the volume fraction profile in Figure 21, the straight channel is initially full of palm oil, which is the continuous phase. At t=0, the methanol enters the inlet and forms a rounded interface once it is in contact with the palm oil phase. The methanol continues traveling along the inlet channel until it reaches the main channel. The methanol slug starts to form at this point and increases in size as it approaches the end of the channel with a very long neck that is not detached. This flow pattern is called irregular slug flow, a breakup phenomenon that leads to a wide distribution of droplet sizes [41].

irregular slug flow is observed at high flow rates of both the dispersed and continuous phases [40,41]. This is applicable in this case, where the methanol flow rate increased from 0.223 m/s (with the 7.6 molar ratio case) to 0.446 m/s. This irregular slug phenomenon is intensely profound in the serpentine microchannels due to the presence of the corners that allow for more slug breakup compared to the straight channel. It was observed that there is some palm oil between the wall and the interface of the slug, the same as the previous microchannel. The flow reaches the end of the channel at t= 1.640s.
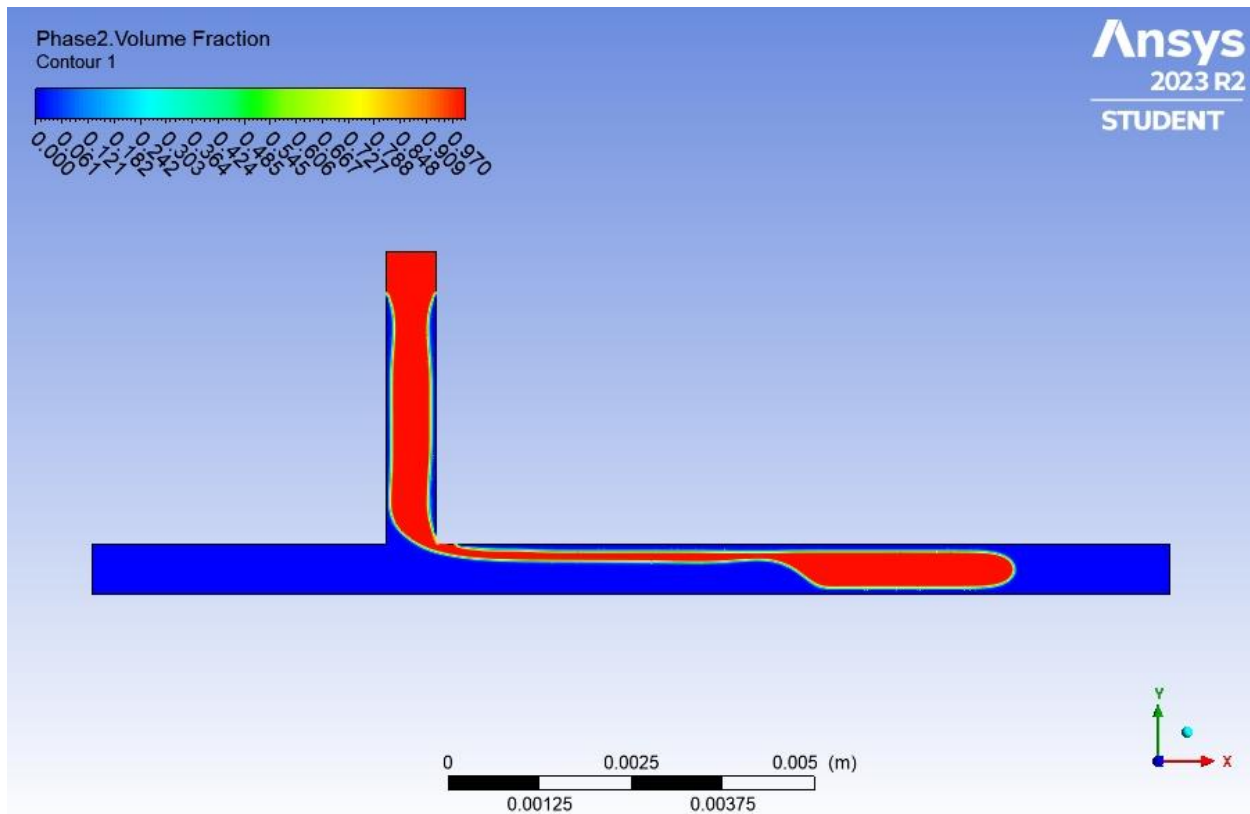
Figure 21 Straight Microchannel VOF Profile for Molar Ratio of 22.9

Serpentine Microchannel with 90-degree Corners and Low Curvature

In the serpentine microchannel with 90-degree corners, the methanol enters the main channel, going downwards in the first unit. Due to a higher molar ratio, it can be observed that the neck breakage happens in the second unit instead of the first, as in the serpentine microchannel with a 7.6 molar ratio. This means there will be a delay in forming slugs in this microchannel with the 22.9 molar ratios. Furthermore, it was noticed that the number of slugs is higher than the 7.6 molar ratio case and not uniform in size. The 22.9 molar ratio generated slugs with a smaller ratio of length to diameter (L/D), and others have a larger L/D ratio. The slug L/D ratio was measured by

an image processing software. Based on the measurements, the slug size was divided into three categories. The first category is when the L/D is less than 2.3, the second category is when the L/D is between 2.3 and 6, and the third category is of the slugs with an L/D larger than 6. The exact impact of the width and corners has been observed on the different slug sizes as with the 7.6 molar ratio. The slug reaches the end of the channel at t= 2.044. In the rounded corners and high curvature serpentine microchannels, as depicted in Figures 23 and 24, the movement of the slug along the channel is the same as the previous 90-degree serpentine microchannel. The same is also observed regarding the slug diameter and length; there are different slugs with different sizes. The slug in the rounded corner and high curvature microchannel reaches the end of the channel at t= 2.047s and t=1.630s respectively.

Figure 22 Serpentine Microchannel with 90-Degree Corners and Low Curvature VOF Profile for Molar Ratio of 22.9

Figure 23 Serpentine Microchannel with Rounded Corners and Low Curvature VOF Profile for Molar Ratio of 22.9

Figure 24 Serpentine Microchannel with 90-Degree Corners and High Curvature VOF Profile for Molar Ratio of 22.9

5.2.2.2 Internal Circulation Streamlines

Internal Circulations Streamlines in Slugs with L/D>6 in the Straight Microchannel

For the straight microchannel, the slug depicted in the figure 25 contains two lengthy major circulations and two minor circulations positioned in the front of the slug. As illustrated in Figure 25, the minor circulations in the rear were stretched, as the rear of the slug was still attached to the neck of the inlet flow. The anticipated vorticity value will be very low within this slug since, there is a very long circulations and a big area of stagnant zones.
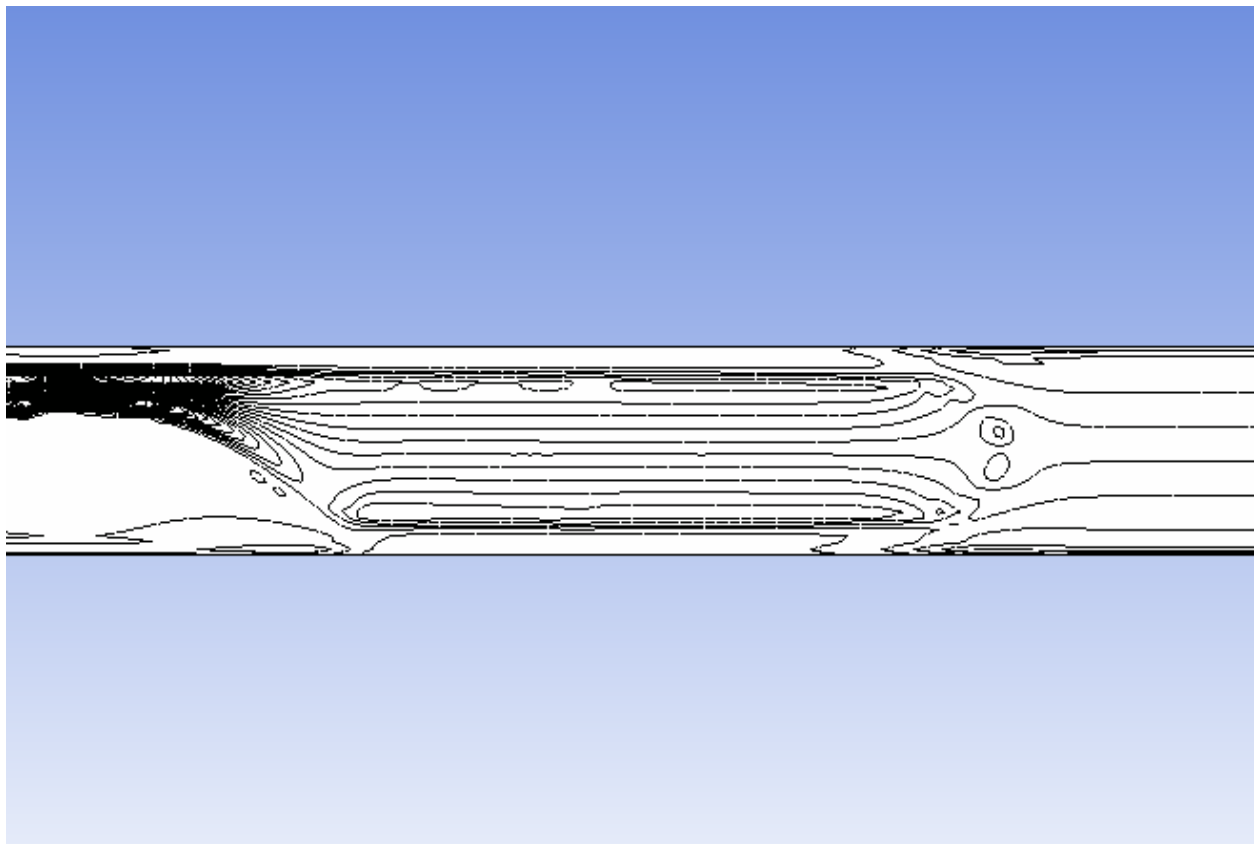
Figure 25 Internal Circulations in Straight Microchannel for Molar Ratio of 22.9

49

Although there are different slug sizes, it was found that all slugs have the same number of circulations as the slugs formed with the 7.6 molar ratio. Two are considered the major circulations, and the other four are the minor ones. All the slugs under these three categories behaved the same as slugs with the 7.6 molar ratio at all of the different segments of the serpentine microchannels: 517.5 µm width segment, 345 µm width segment, and the corners. It is worth noting that as the L/D ratio increases, the length of the major circulation also increases; this is depicted clearly with the L/D>6 slug in Figure 26D.
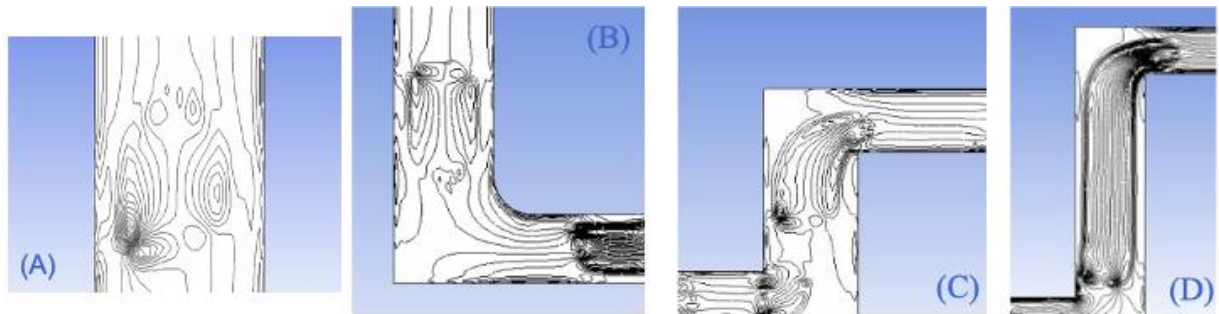
Figure 26 Internal Circulations in different slug sizes (A) L/D<2.3, (B) 2.3<L/D<6, (C) 2.3<L/D<6, (D) L/D>6 for Molar Ratio of 22.9 in different serpentine microchannel configurations

It was perceived, as depicted in the following Figures 27, 28, 29, and 30, that the same major circulation movement was observed in all the slug sizes. The left half of circulation moves counterclockwise, while the right half of major circulation moves clockwise.
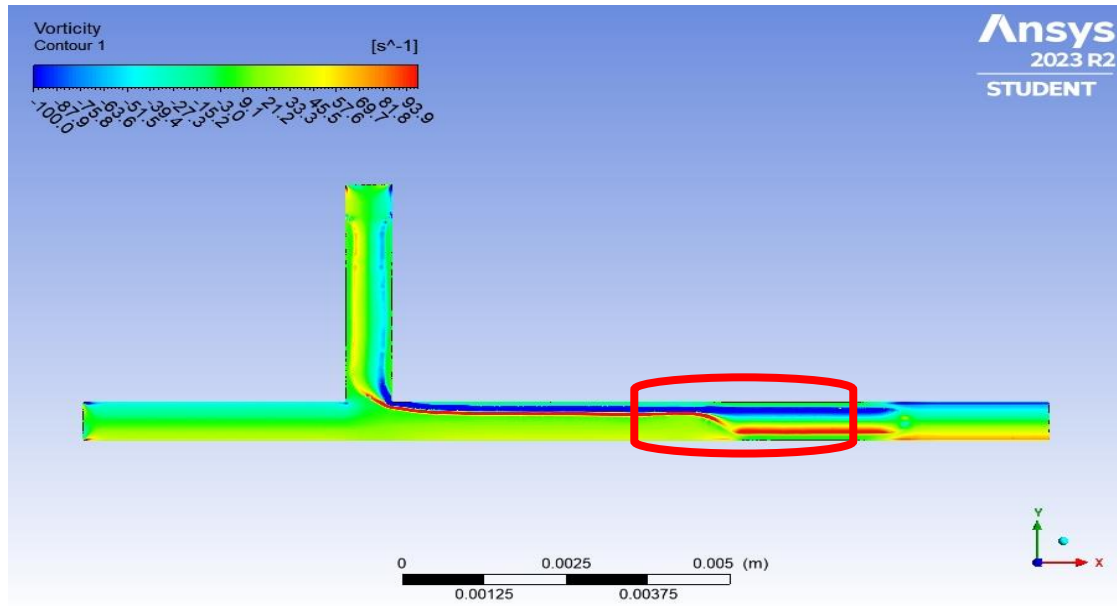
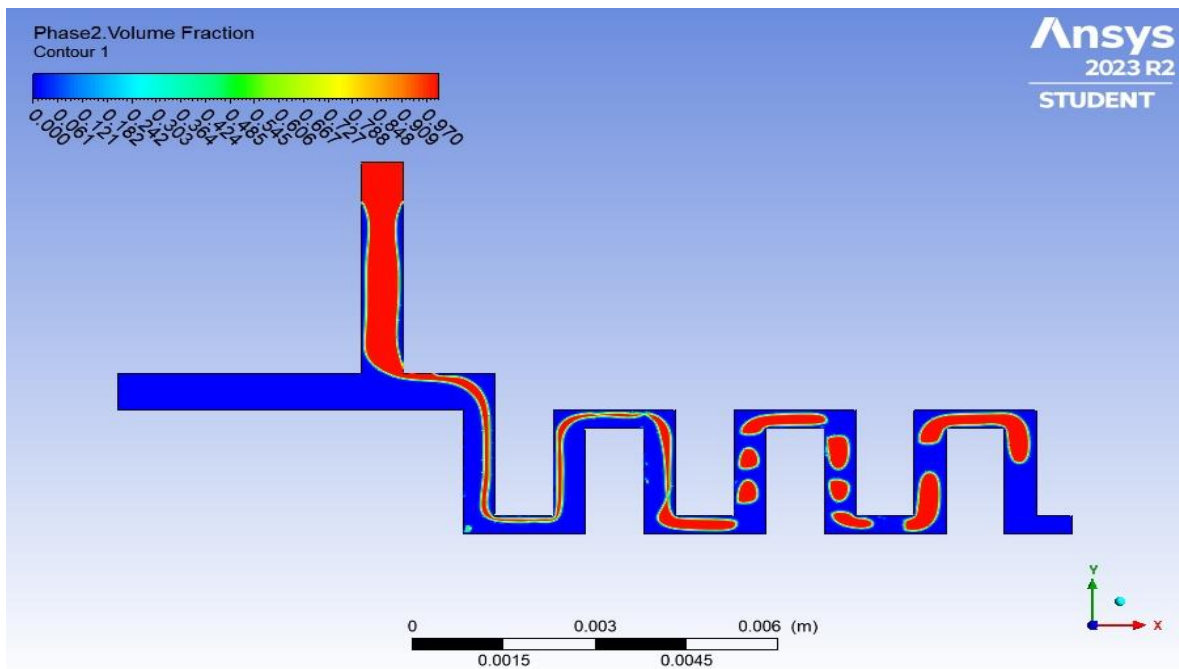*Figure 27 Straight Microchannel Vorticity Contour for Molar Ratio of 22.9*
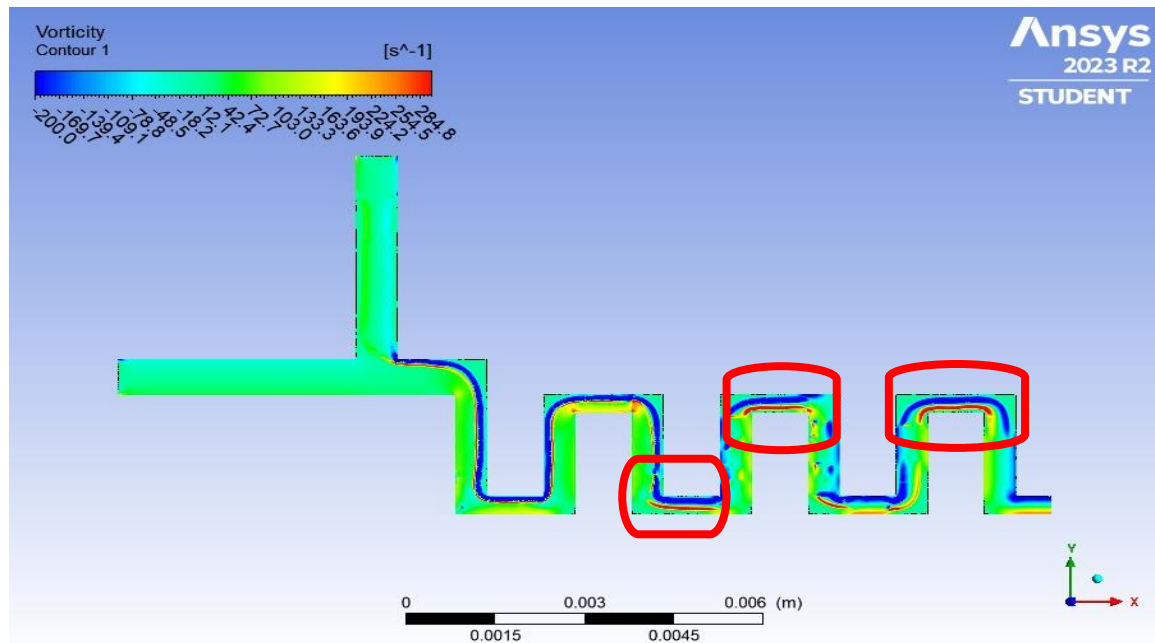
Figure 28 Serpentine Microchannel with 90-Degree Corners and Low Curvature Vorticity Contour for Molar ratio of 22.9
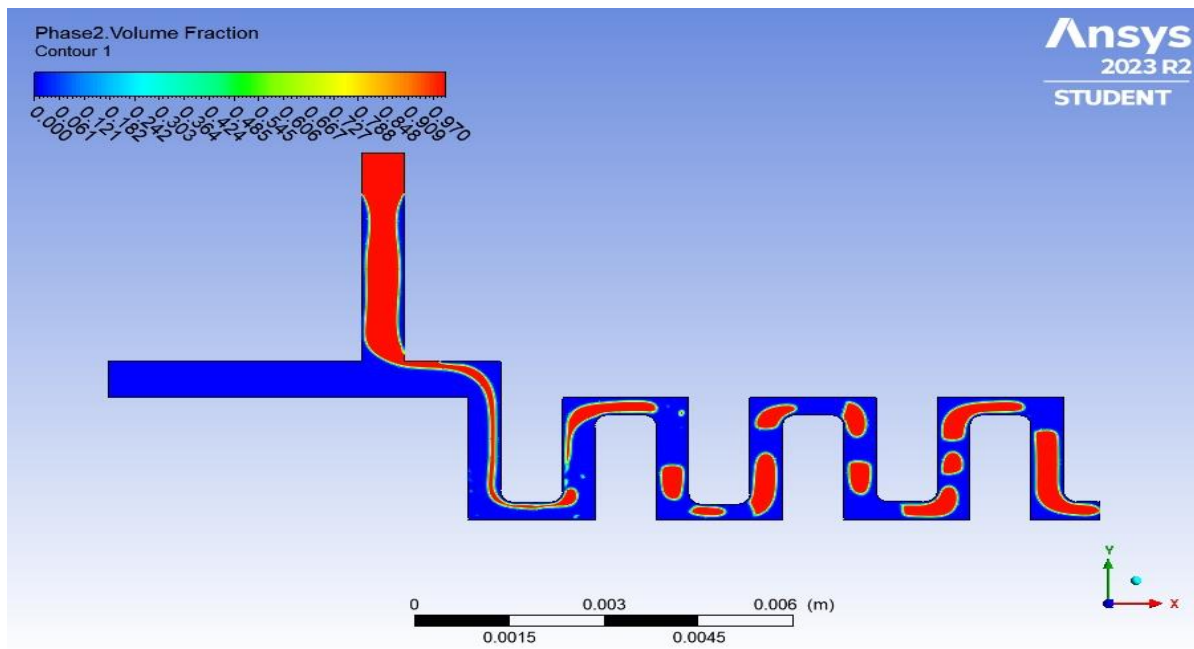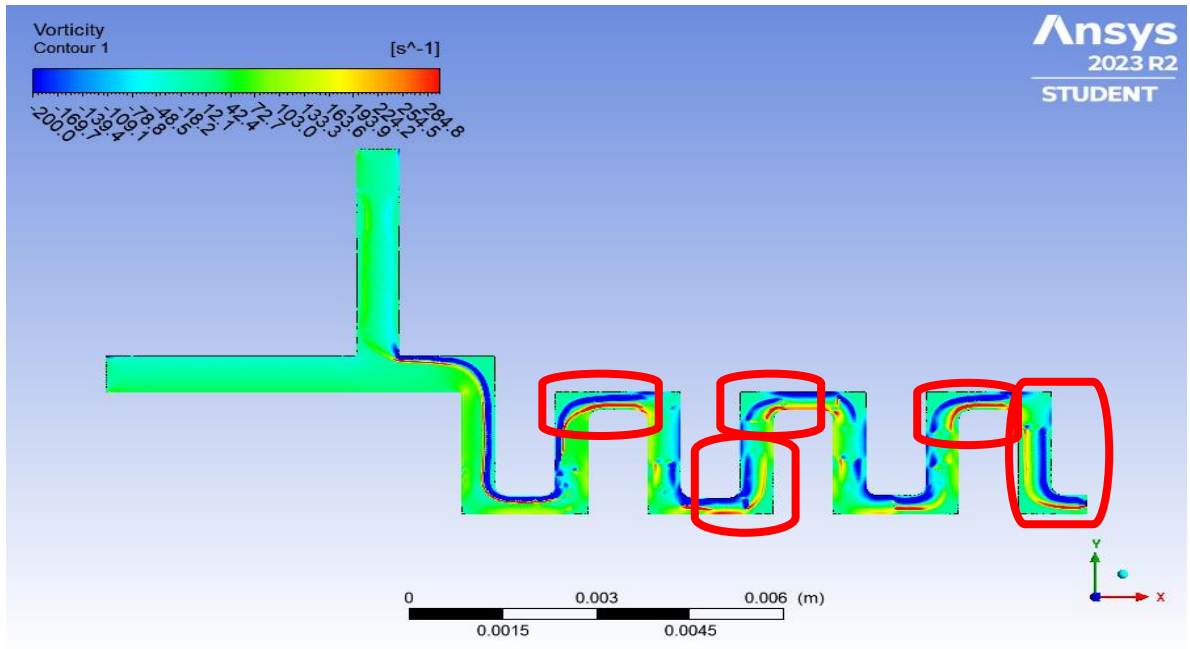
Figure 29 Serpentine Microchannel with Rounded Corners and Low Curvature Vorticity Contour for Molar ratio of 22.9
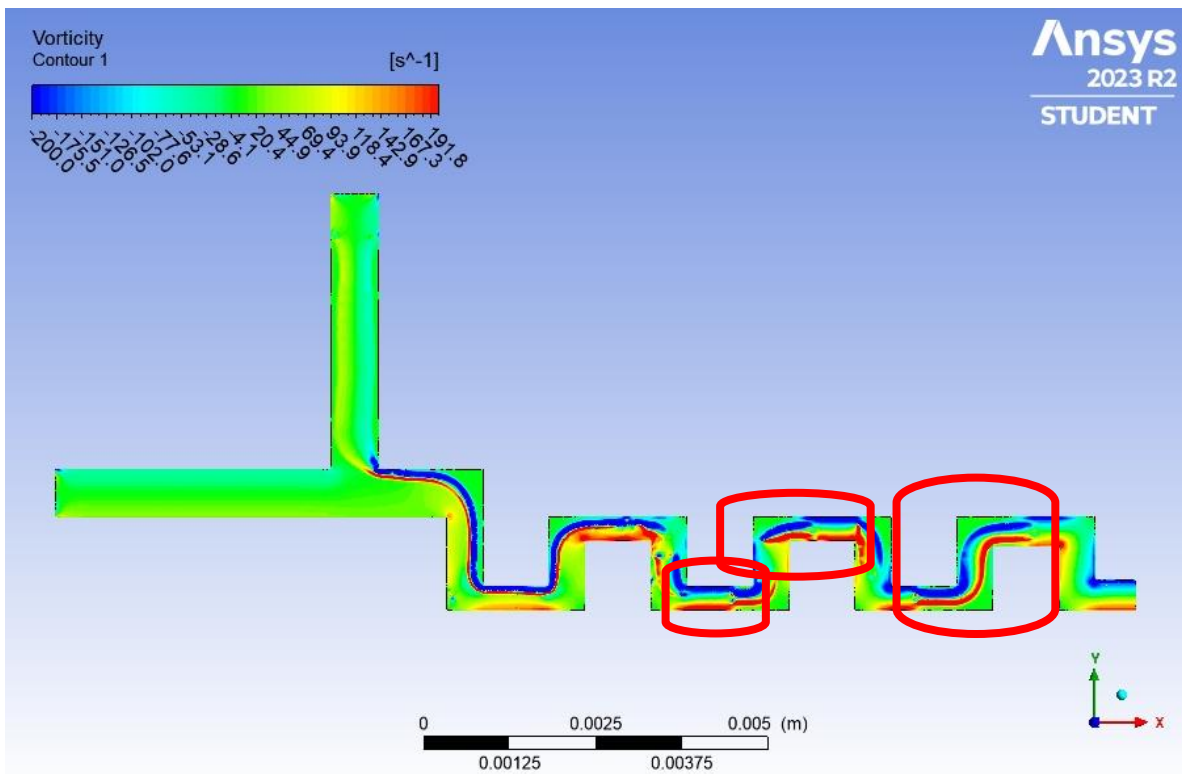
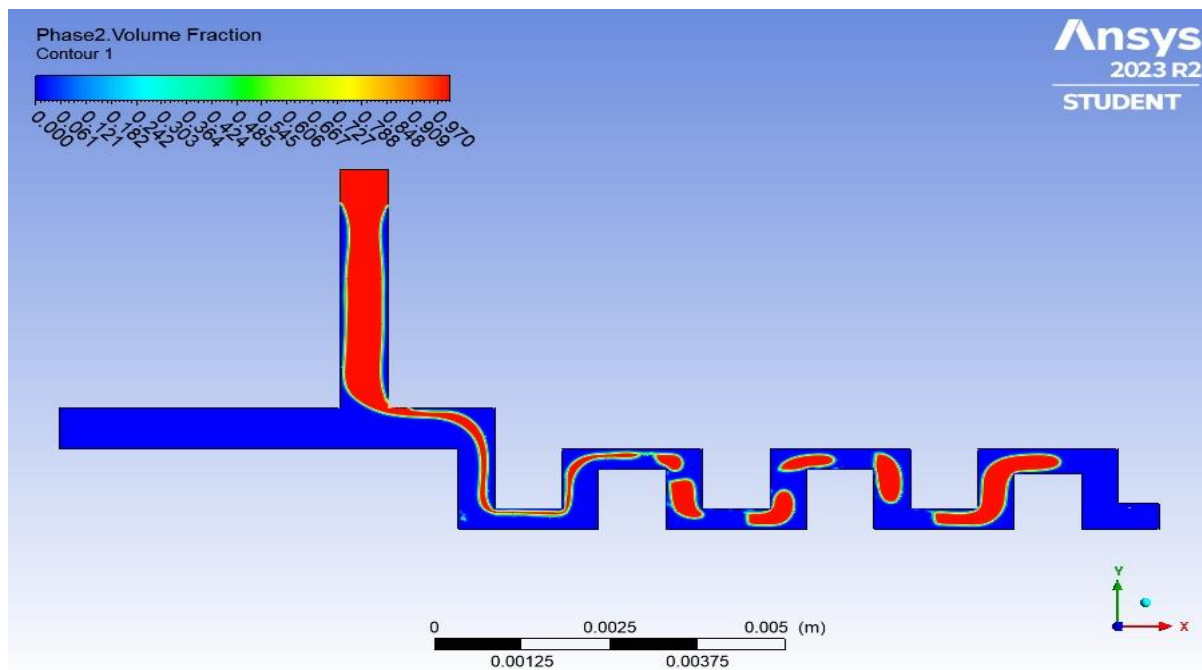*Figure 30 Serpentine Microchannel with 90-Degree Corners and High Curvature Vorticity Contour for Molar ratio of 22.9*

5.2.2.3 Vorticity Measurement

As discussed earlier, the 22.9 molar ratio resulted in different slug sizes. Therefore, it was decided to study the impact of the slug sizes on vorticity for the serpentine microchannel with 90-degree and low curvature. Figure 31 found that the slug with L/D > 6 induced the lowest vorticities, especially in the 517.5µm width segment. This is due to the lengthy major internal circulations and the stagnant zone's growth, leading to the decline of interface renewal and mass transfer when it comes to mixing [42]. It was also noticed that the vorticity enhanced significantly when the slugs with L/D > 6 moved around the bends and through the 345 µm width segment. Regarding the L/D < 2.3 slugs, the vorticity was found to be better than the L/D > 6 slug in almost all locations. Also, the positive impact of the bends is evident on the L/D < 2.3 slug; the bend significantly strengthened the vorticity. The only demerit with this slug size is that the short diffusion length provided by the short internal circulations might not be enough for complete mixing time, so there is not enough time for substances to spread throughout the mixture to achieve complete mixing. The 2.3 < L/D < 6 slug was the optimum slug size that resulted in the highest vorticity among the other two size categories.

The most likely slug size to achieve the highest mixing efficiency is the slug size of L/D between 2.3 and 6. Tice et al. (2003) studied the impact of changing flow rates on mixing inside aqueous slug in a straight microchannel [43], and their results showed that the maximum mass transfer efficiency was achieved when the dispersed phase fraction was close to 0.3. The slug size of L/D between 2.3 and 6 is associated with a dispersed phase fraction of 0.25; therefore, it is possible to anticipate high mass transfer achieved through this slug size. However, it is believed that all the

other slug sizes can also obtain high mixing efficiency due to the vorticity rise triggered by the bends, which is very close in all the slug sizes.
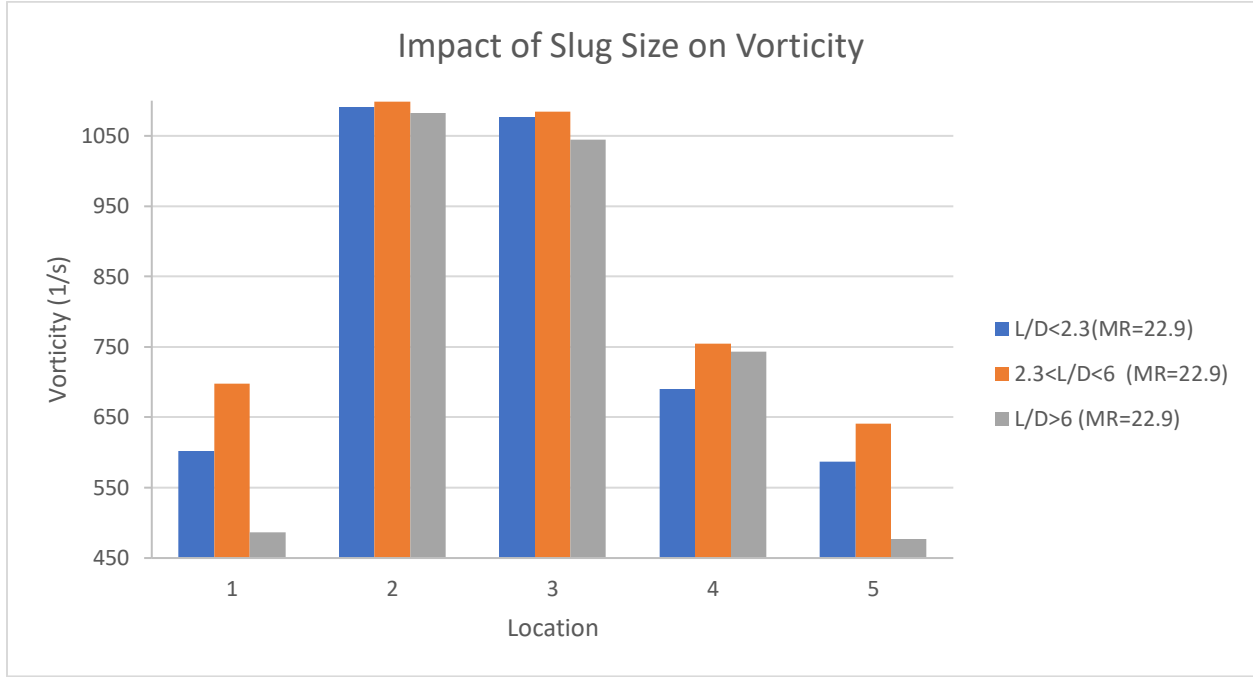
Figure 31 Impact of Slug Size on Vorticity

When comparing the molar ratio of 7.6 to 22.9 for the same slug size ($2.3 < L/D < 6$), it was found that there is no significant difference in vortices, which makes sense since the slug size is in the same range and no microchannel geometry differences for both molar ratios. Therefore, the vorticity in this case will be omitted in the selection criteria, and the number of slugs in each case, as well as the stability of the flow pattern, will be used as part of the criteria. Obviously, the 7.6 molar ratio is a good selection when it comes to flow stability (i.e., uniformed slug size) since it is more stable when compared to the 22.9, which will lead to easier operations of the microchannel. Moreover, the number of $2.3<L/D<6$ slugs with the 7.6 molar ratios is higher by 20% than the number of slugs for the 22.9 case, which again looks like a better choice than the 22.9 molar ratio.

Nevertheless, considering all the slug sizes, the 22.9 molar ratio would be a better choice if higher throughput is more critical to the operations because the slug total number (of all sizes) and velocity in the 22.9 is higher than the 7.6 molar ratio.
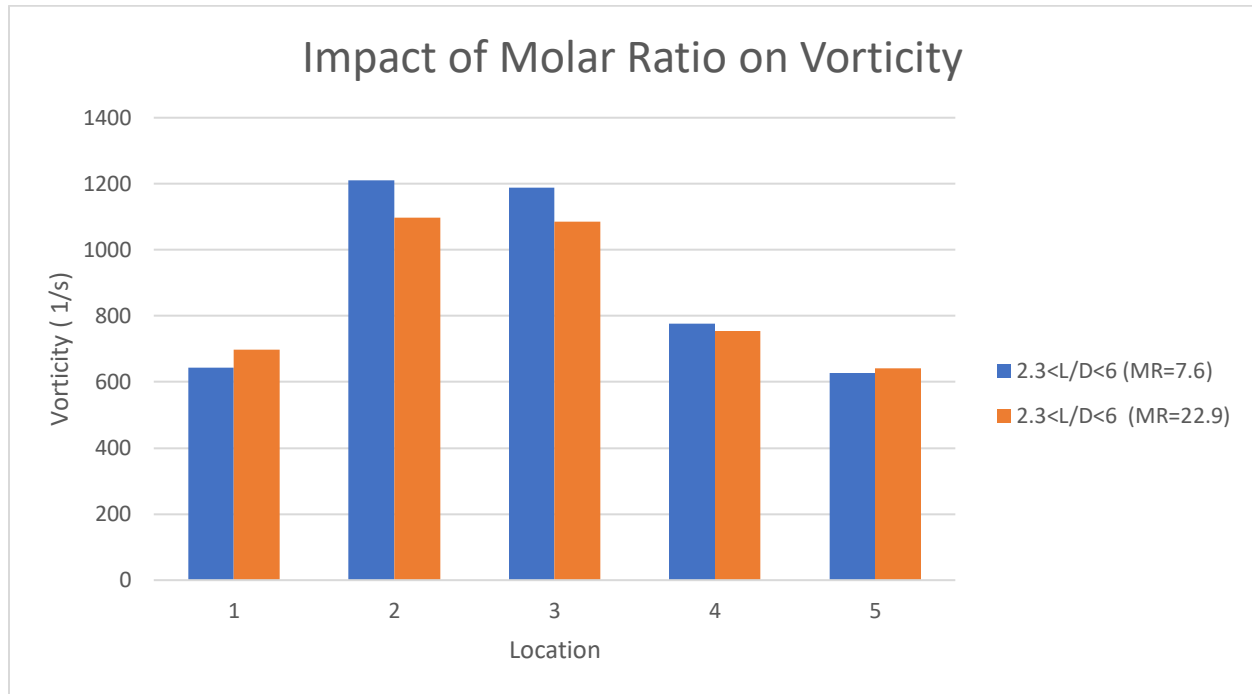
Figure 32 Impact of Molar Ratio on Vorticity

Chapter 6: Conclusion and Future Work

In this study, the hydrodynamics of slug flow patterns in various serpentine microchannels were numerically investigated to enhance biodiesel production using the Volume of Fluid (VOF) method. Additionally, a straight microchannel was simulated to compare the impact of geometry configuration on vorticity. When examining serpentine microchannels, the study considered the impact of geometrical factors like width, corner shape, and curvature radius, along with operational parameters such as the alcohol-to-oil ratio, in order to optimize microchannel performance. The results demonstrated that serpentine microchannels achieved significantly higher vorticity, with narrower widths proving to be more advantageous. Furthermore, a 90-degree corner shape induced slightly higher vorticity compared to a rounded shape due to increased deformations within the internal circulations resulting from the sharp intrusion. Longer curvature radius also contributed to improved vorticity, while a very short radius caused excessive deformation of the internal circulation, leading to reduced vorticity. Lastly, in terms of molar ratios, the 7.6 molar ratio resulted in a higher number of slugs falling within the L/D range of 2.3 to 6 compared to the 22.9 molar ratio. This specific L/D range was associated with the highest vorticity compared to other ranges (L/D<2.3 and L/D>6) when considering the 22.9 molar ratio.

As for future work, the study can be backed up by including a transport species model in the simulation to relate the vorticity enhancement due to the serpentine microchannel configurations with the mixing efficiency. Moreover, although the system was already validated, including the experimental work specifically for the serpentine microchannels would improve the system's

certainty. Also, including a wide range of curvature radius would be more reasonable to prove that the radius does not have to be very short to increase the vorticity and, consequently, the mixing as per the Dean Number.

References

[1] Eslam G. A., Mohammed G. M., Alaaeldin A. E. "Comparison between biodiesel production from vegetable oils and waste cooking oils" Frontiers in Energy Research, Vol 8, pp. 278 –291, 2020.

[2] Widayat, A. D. Wibowo, and Hadiyanto, "Study on Production Process of Biodiesel from Rubber Seed (Hevea Brasiliensis) by in Situ (Trans)Esterification Method with Acid Catalyst," Energy Procedia, vol. 32, pp. 64–73, 2013.

[3] E. López-Guajardo, E. Ortiz-Nadal, A. Montesinos-Castellanos, and K. D. Nigam, "Process Intensification of Biodiesel Production Using a Tubular Micro-Reactor (TMR): Experimental and Numerical Assessment," Chemical Engineering Communications, vol. 204, no. 4, pp. 467–475, 2017.

[4] Y. Natarajan, A. Nabera, S. Salike, V. Dhanalakshmi Tamilkkuricil, S. Pandian, M. Karuppan, and A. Appusamy, "An overview on the process intensification of microchannel reactors for biodiesel production," Chemical Engineering and Processing - Process Intensification, vol. 136, pp. 163–176, 2019.

[5] Kingsley Chilakpu, Godfrey Nwandikom, Sabbas Asoegwu, and C. C. Egwuonwu, "Modification of Biodiesel Batch Reactor," Emerging Trends in Engineering and Applied Sciences, pp. 262–264 , 2014.

[6] D. O. M. I. N. I. Q. U. E. M. ROBERGE and MICHAEL GOTTSPONER, "Industrial design, scale-up, and use of microreactors," Chemistry Today, vol. 27, pp. 8–11, 2009.

[7] H. S. Santana, D. S. Tortola, J. L. Silva, and O. P. Taranto, "Biodiesel synthesis in micromixer with static elements," Energy Conversion and Management, vol. 141, pp. 28–39, 2017.

[8] T. Neadkratoke, "Numerical simulation of biodiesel synthesis in a continuous flow microreactor and a porous media reactor," Ph.D. Dissertation, The university of texas., Arlington, 2019.

[9] W. Han, R. Charoenwat, and B. H. Dennis, "Numerical Investigation of Biodiesel Production in Capillary Microreactor," Volume 2: 31st Computers and Information in Engineering Conference, Parts A and B, 2011.

[10] Mohd Laziz, A. et al. (2020) 'Rapid production of biodiesel in a microchannel reactor at room temperature by enhancement of mixing behaviour in methanol phase using volume of fluid model', Chemical Engineering Science, 219, p. 115532. doi:10.1016/j.ces.2020.115532.

[11] A. Mohd Laziz, K. KuShaari, J. Chin, and J. Denecke, "Quantitative analysis of hydrodynamic effect on transesterification process in T-junction microchannel reactor system," Chemical Engineering and Processing - Process Intensification, vol. 140, pp. 91–99, 2019. doi:10.1016/j.cep.2019.04.019

[12] C. Chen, Y. Zhao, J. Wang, P. Zhu, Y. Tian, M. Xu, L. Wang, and X. Huang, "Passive Mixing inside Microdroplets," Micromachines, vol. 9, no. 4, p. 160, 2018.

[13] J. Wang, J. Wang, L. Feng, and T. Lin, "Fluid mixing in droplet-based microfluidics with a serpentine microchannel," RSC Advances, vol. 5, no. 126, pp. 104138–104144, 2015.

[14] M. Madadelahi and A. Shamloo, "Droplet-based flows in serpentine microchannels: Chemical reactions and secondary flows," International Journal of Multiphase Flow, vol. 97, pp. 186–196, 2017.

[15] J.-yuan Qian, X.-juan Li, Z.-xin Gao, and Z.-jiang Jin, "Mixing efficiency and pressure drop analysis of liquid-liquid two phases flow in serpentine microchannels," Journal of Flow Chemistry, vol. 9, no. 3, pp. 187–197, 2019.

[16] X. Cao, B. Zhou, C. Yu, and X. Liu, "Droplet-based mixing characteristics in bumpy serpentine microchannel," Chemical Engineering and Processing - Process Intensification, vol. 159, p. 108246, 2021.

[17] Ansys fluent | Fluid Simulation Software, https://www.ansys.com/products/fluids/ansys-fluent (accessed Oct. 6, 2023).

[18] Hirt, C.W. and Nichols, B.D. (1981) 'Volume of fluid (VOF) method for the dynamics of Free Boundaries', Journal of Computational Physics, 39(1), pp. 201–225. doi:10.1016/0021-9991(81)90145-5.

[19] M. Athar and S. Zaidi, "A review of the feedstocks, catalysts, and intensification techniques for Sustainable Biodiesel production," Journal of Environmental Chemical Engineering, vol. 8, no. 6, p. 104523, 2020. doi:10.1016/j.jece.2020.104523

[20] Qamareen, A., Ansari, M.A. and Alam, S.S. (2022) 'Mixing enhancement using the aiding and opposing flow effects in Curved Micro Channel', Chemical Engineering and Processing - Process Intensification, 176, p. 108945. doi:10.1016/j.cep.2022.108945.

[21] Tung, K.-Y., Li, C.-C. and Yang, J.-T. (2009) 'Mixing and hydrodynamic analysis of a droplet in a planar serpentine micromixer', Microfluidics and Nanofluidics, 7(4), pp. 545–557. doi:10.1007/s10404-009-0415-8.

[22] D. Tsaoulidis and P. Angeli, "Effect of channel size on liquid-liquid plug flow in small channels," AIChE Journal, vol. 62, no. 1, pp. 315–324, 2015. doi:10.1002/aic.15026

[23] Q. Zhang, H. Liu, S. Zhao, C. Yao, and G. Chen, "Hydrodynamics and mass transfer characteristics of liquid–liquid slug flow in microchannels: The effects of temperature, fluid properties and channel size," Chemical Engineering Journal, vol. 358, pp. 794–805, 2019. doi:10.1016/j.cej.2018.10.056

[24] N. Di Miceli Raimondi, L. Prat, C. Gourdon, and P. Cognet, "Direct numerical simulations of mass transfer in square microchannels for liquid–liquid slug flow," Chemical Engineering Science, vol. 63, no. 22, pp. 5522–5530, 2008. doi:10.1016/j.ces.2008.07.025

[25] Q. Li and P. Angeli, "Experimental and numerical hydrodynamic studies of ionic liquid-aqueous plug flow in small channels," Chemical Engineering Journal, vol. 328, pp. 717–736, 2017. doi:10.1016/j.cej.2017.07.037

[26] Y. Han and N. Shikazono, "Measurement of the liquid film thickness in micro tube slug flow," International Journal of Heat and Fluid Flow, vol. 30, no. 5, pp. 842–853, Oct. 2009, doi: https://doi.org/10.1016/j.ijheatfluidflow.2009.02.019.

[27] V. Srinivasan and S. Khandekar, "Thermo-hydrodynamic transport phenomena in partially wetting liquid plugs moving inside micro-channels," Sadhana-academy Proceedings in Engineering Sciences, vol. 42, no. 4, pp. 607–624, Mar. 2017, doi:https://doi.org/10.1007/s12046-017-0618-8.

[28] M. N. Kashid and D. W. Agar, "Hydrodynamics of liquid–liquid slug flow capillary microreactor: Flow regimes, slug size and pressure drop," Chemical Engineering Journal, vol. 131, no. 1–3, pp. 1–13, Jul. 2007, doi: https://doi.org/10.1016/j.cej.2006.11.020.

[29] A. Marty, C. Causserand, C. Roques, and P. Bacchin, "Impact of tortuous flow on bacteria streamer development in microfluidic system during filtration," Biomicrofluidics, vol. 8, no. 1, Jan. 2014, doi: https://doi.org/10.1063/1.4863724.

[30] Z. Che, Teck Neng Wong, and N. Nguyen, "Heat transfer in plug flow in cylindrical microcapillaries with constant surface heat flux," International Journal of Thermal Sciences, vol. 64, pp. 204–212, Feb. 2013, doi: https://doi.org/10.1016/j.ijthermalsci.2012.09.006.

[31] R. Antony, M. S. Giri Nandagopal, N. Sreekumar, S. Rangabhashiyam, and N. Selvaraju, "Liquid-liquid Slug Flow in a Microchannel Reactor and its Mass Transfer Properties - A Review," Bulletin of Chemical Reaction Engineering & Catalysis, vol. 9, no. 3, Oct. 2014, doi: https://doi.org/10.9767/bcrec.9.3.6977.207-223.

[32] P. Bayat and P. Rezai, "Semi-Empirical Estimation of Dean Flow Velocity in Curved Microchannels," Scientific Reports, vol. 7, no. 1, Oct. 2017, doi: https://doi.org/10.1038/s41598-017-13090-z.

[33] L. Lei, Y. Zhao, X. Wang, G. Xin, and J. Zhang, "Experimental and numerical studies of liquid-liquid slug flows in micro channels with Y-junction inlets," Chemical Engineering Science, vol. 252, p. 117289, Apr. 2022, doi: https://doi.org/10.1016/j.ces.2021.117289.

[34] Özkan A, Erdem EY (2015) Numerical analysis of mixing performance in sinusoidal microchannels based on particle motion in droplets. Microfluid Nanofluid 19:1101–1108. https://doi.org/10.1007/ s10404-015-1628-7

[35] Sattari-Najafabadi M, Esfahany N, Wu Z, Sundén B (2017b) The effect of the size of square microchannels on hydrodynamics and mass transfer during liquid-liquid slug flow. AIChE J 63:5019–5028. https://doi.org/10.1002/aic.15822

[36] T. Rhoades, C. R. Kothapalli, and P. S. Fodor, "Mixing Optimization in Grooved Serpentine Microchannels," Micromachines, vol. 11, no. 1, p. 61, Jan. 2020, doi: https://doi.org/10.3390/mi11010061.

[37] J. Qian, X. Li, Z. Gao, and Z. Jin, "Mixing efficiency and pressure drop analysis of liquid-liquid two phases flow in serpentine microchannels," Journal of Flow Chemistry, vol. 9, no. 3, pp. 187–197, Jun. 2019, doi: https://doi.org/10.1007/s41981-019-00040-1.

[38] R. K. Verma and S. Ghosh, "Curvature induced intensification of biodiesel synthesis in miniature geometry," Chemical Engineering and Processing - Process Intensification, vol. 163, p. 108363, Jun. 2021, doi: https://doi.org/10.1016/j.cep.2021.108363.

[39] J. Qian, X. Li, Z. Wu, Z. Jin, and B. Sunden, "A comprehensive review on liquid–liquid two-phase flow in microchannel: flow pattern and mass transfer," Microfluidics and Nanofluidics, vol. 23, no. 10, Sep. 2019, doi: https://doi.org/10.1007/s10404-019-2280-4.

[41] R. Prakash, Raj Kumar Verma, and S. Ghosh, "Liquid-liquid mass transfer in a serpentine miniature geometry- effect on pressure drop," Chemical Engineering Journal, vol. 369, pp. 489–497, Aug. 2019, doi: https://doi.org/10.1016/j.cej.2019.03.064.

[40] C. Liu, Q. Zhang, C. Zhu, T. Fu, and H. Z. Li, "Formation of droplet and 'string of sausages' for water-ionic liquid ([BMIM][PF6]) two-phase flow in a flow-focusing device," Chemical Engineering and Processing - Process Intensification, vol. 125, pp. 8–17, Mar. 2018, doi: https://doi.org/10.1016/j.cep.2017.12.017.

[42] Sattari-Najafabadi M, Esfahany MN, Wu Z, Sundén B (2017a) Hydro- dynamics and mass transfer in liquid-liquid non-circular micro- channels: comparison of two aspect ratios and three junction structures. Chem Eng J 322:328–338. https://doi.org/10.1016/j. cej.2017.04.028

[43] Tice JD, Song H, Lyon AA, Ismagilov RF (2003) Formation of drop-lets and mixing in multiphase microfluidics at low values of the Reynolds and the capillary numbers. Langmuir 19:9127–9133. https://doi.org/10.1021/la030090w

Appendices

Appendix A: Volumetric Flowrate Calculations for Each Molar Ratio

Table 6 Volumetric Flowrate Calculations for 7.6 Molar Ratio

Total Volumetric Flowrate	0.2	ml/min	200
Reactants		Methanol	Oil
Molar Ratio	mol/min	= 7.6	= 1
Molecular weight	g/moles	= 32.040	= 845.910
Mass Flowrate	g/min	= 7.6 * 32.040 = 243.504	= 845.910 * 1 = 845.91
Density	g/ m^3	785000	909000
Volumetric Flowrate for Each Phase	m^3/min	= 243.504 / 785000 = 0.000310	= 845.91 / 909000 = 0.000930
Volumetric Flowrate for Each Phase	ml/min	= 0.000310 * 1000000 = 310.000	= 0.000930 * 1000000 = 930.000
Volume Fraction		= 310.000 / (310.000 + 930.000) = 0.250	= 930.000 / (310.000 + 930.000) = 0.750
Volumetric Flowrate for Each Phase (after scaling)	ml/min	= 0.2 * 0.250 = 0.0499	= 0.2 * 0.750 = 0.150
Volumetric Flowrate for Each Phase (after scaling)	µL/min	= 0.0499 * 1000 = 49.999	= 0.150 * 1000 = 150.000

Table 7 Volumetric Flowrate Calculations for 22.9 Molar Ratio

Total Volumetric Flowrate	0.2	ml/min	200
Reactants		Methanol	Oil
Molar Ratio	mol/min	22.9	1
Molecular weight	g/moles	32.040	845.910
Mass Flowrate	g/min	= 22.9 * 32.040 = 733.716	= 845.910 * 1 = 845.910
Density	g/m^3	785000	909000
Volumetric Flowrate for Each Phase	m^3/min	= 733.716/ 785000 = 0.935	= 845.910/ 909000 = 0.931
Volumetric Flowrate for Each Phase	ml/min	= 0.935 * 1000000 = 935	= 0.931 * 1000000 = 931
Volume Fraction		= 935 / (935 + 931) = 0.5	= 931 / (935 + 931) = 0.5
Volumetric Flowrate for Each Phase (after scaling)	ml/min	= 0.2 * 0.5 = 0.100	= 0.2 * 0.5 = 0.100
Volumetric Flowrate for Each Phase (after scaling)	µL/min	= 0.100 * 1000 = 100.000	= 0.100 * 1000 = 100.000

Appendix B: Dean Number Calculations

Serpentine Microchannel with Constant Width

$$D = L$$

$$R = L + \frac{L}{2} = \frac{3L}{2}$$

$$R_e = \frac{\rho \cdot v \cdot L}{\mu}$$

$$\sqrt{\frac{D}{R}} = \sqrt{\frac{1L}{\frac{3L}{2}}} = 0.82$$

$$D_e = 0.82 \cdot \frac{\rho \cdot v \cdot L}{\mu}$$

Serpentine Microchannel with Varying Width

$$D = \frac{\left(\frac{3L}{4} + \frac{L}{2}\right)}{2} = \frac{5L}{8}$$

$$R = \frac{\left(\left(\left(\frac{1}{2} \cdot \frac{L}{2}\right) + \frac{36L}{25}\right) + \left(\left(\frac{1}{2} \cdot \frac{3L}{4}\right) + \frac{7L}{10}\right)\right)}{2} = \frac{277L}{200}$$

$$When\ D = L, \qquad v = V_1$$

Using $Q = AV$ & $A_1V_1 = A_2V_2$ since Q is constant while assuming square cross section

$$When\ D = \frac{3L}{4}, \qquad V_2 = \frac{177V_1}{100}$$

$$When\ D = \frac{L}{2}, \qquad V_2 = 4V_1$$

Taking avergae of velocities in both sections $\left(i.e\ section\ with\ ID = \dfrac{3L}{4}\ \&\ ID = \dfrac{L}{2}\right)$

$$V_{avg} = \frac{\left(\dfrac{177v}{100} + 4v\right)}{2} = \frac{72}{25}v$$

$$R_e = \frac{\rho \cdot \dfrac{72}{25}v \cdot \dfrac{5}{8}L}{\mu}$$

$$\sqrt{\frac{D}{R}} = \sqrt{\frac{\dfrac{5L}{8}}{\dfrac{277L}{200}}} = 0.672$$

$$D_e = 0.672 \cdot \frac{\rho \cdot \dfrac{72}{25}v \cdot \dfrac{5}{8}L}{\mu} = 1.2 \ \cdot \frac{\rho \cdot v \cdot L}{\mu}$$

Appendix C: Bend Ratio Calculations for 90-degree and Rounded Corners

90-degree corner:

$$R = \frac{Average\ Channel\ Width\ W}{Raduis\ of\ the\ Bend} = \frac{W_{avg}}{R_B} = \frac{\left(\dfrac{517.5 + 345}{2}\right)}{0} = Undefined$$

Rounded Corner (Bend Diameter = 400µm):

$$R = \frac{Average\ Channel\ Width\ W}{Raduis\ of\ the\ Bend} = \frac{W_{avg}}{R_B} = \frac{\left(\dfrac{517.5 + 345}{2}\right)}{200 + \left(\dfrac{1}{2} \cdot \dfrac{517.5 + 345}{2}\right)} = 1.03$$

All dimensions in µm.